Yichao Zeng
Department of Industrial and Manufacturing Systems Engineering, University of Michigan-Dearborn, 4901 Evergreen Rd Dearborn, MI 48128, US
email: zyichao@umich.edu

Zhao Zhao
Department of Industrial and Manufacturing Systems Engineering, University of Michigan-Dearborn, 4901 Evergreen Rd Dearborn, MI 48128, US
email: zhaozhao@umich.edu

Guofeng Qian
Department of Structural Engineering, University of California San Diego, 9500 Gilman Drive Mail Code 0085 La Jolla, CA 92093 email: g4qian@ucsd.edu

Michael D. Todd
Department of Structural Engineering, University of California San Diego, 9500 Gilman Drive Mail Code 0085 La Jolla, CA 92093 email: mdtodd@ucsd.edu

Zhen Hu[1]
Department of Industrial and Manufacturing Systems Engineering, University of Michigan-Dearborn, 4901 Evergreen Rd Dearborn, MI 48128, US
email: zhennhu@umich.edu

Enhancing Bayesian Inference-Based Damage Diagnostics Through Domain Translation with Application to Miter Gates

Bayesian inference based on computational simulations plays a crucial role in model-informed damage diagnostics and the design of reliable engineering systems, such as the miter gates studied in this paper. While Bayesian inference for damage diagnostics has shown success in some applications, the current method relies on monitoring data from solely the asset of interest and may be affected by imperfections in the computational simulation model. To address these limitations, this paper introduces a novel approach called Bayesian Inference-based Damage Diagnostics Enhanced through Domain Translation (BiEDT). The proposed BiEDT framework incorporates historical damage inspection and monitoring data from similar yet different miter gates, aiming to provide alternative data-driven methods for damage diagnostics. The proposed framework first translates observations from different miter gates into a unified analysis domain using two domain translation techniques, namely CycleGAN and Domain-Adversarial Neural Network (DANN). Following the domain translation, a conditional invertible neural network (cINN) is employed to estimate the damage state, with uncertainty quantified in a Bayesian manner. Additionally, a Bayesian model averaging and selection method is developed to integrate the posterior distributions from different methods and select the best model for decision-making. A practical miter gate structural system is employed to demonstrate the efficacy of the BiEDT framework. Results indicate that the alternative damage diagnostics approaches based on domain translation can effectively enhance the performance of Bayesian inference-based damage diagnostics using computational simulations.

Keywords: Bayesian Inference, Domain Translation, Structural Health Monitoring, Damage Detection, Miter Gates

1 Introduction

The US Army Corps of Engineers (USACE) operates numerous inland waterway infrastructure systems, such as navigation locks, at 236 sites across 191 locations. These locks are essential assets for facilitating the transportation of barges and goods from coastal regions to inland regions, which is critical for the national economic security of the United States [1]. Among the miter gates managed by USACE, many of them have exceeded their 50-year design life, which raises concerns about their safety and reliability [1]. As USACE continues to address the challenges of its aging infrastructure, routine evaluations of structural integrity become essential to preemptively identify potential failures and implement timely interventions [2]. This is of paramount importance for reducing unexpected shutdowns and confirming that planned maintenance and repairs are both needed and effective [1,3]. The typical approach to inspecting and monitoring lock components involved shutting down the lock for visual assessments by expert elicitation (trained inspectors). This process is not only labor-intensive but also economically expensive, inefficient, and inconsistent [4].

As a structural integrity assessment and health management tool, structural health monitoring (SHM) and management methods have continued to gain wider acceptance and significance globally in the past decades [5,6]. A well-designed SHM system offers significant advantages, including reduced ownership costs through data-driven maintenance decisions, enhanced operational performance, and minimized risks of catastrophic failures, thereby increasing overall safety [7–9]. To address reliability concerns and maintain operational integrity and safety, USACE started to implement SHM technologies, such as SMART Gate, on inland waterway civil infrastructures [2]. For instance, at the Dalles Navigation Lock, Oregon, the miter gate downstream and the tainter gate upstream have been used for over 50 years. In 2007, inspections identified significant issues like cracking and misalignment, leading to the adoption of SMART Gate technology to monitor and analyze these conditions [10]. By 2009, detected anomalies through SHM system using SMART Gate prompted emergency interventions, including inspection dives and remote operations, culminating in crucial repairs that averted a potential disaster [10].

While SHM plays a vital role in ensuring structure integrity and safety, it requires a rigorous design and implementation approach to fully materialize its benefits [11]. Various approaches have been developed to enable effective damage diagnostics and failure prognostics in SHM. Amongst all available approaches, one of the most commonly used SHM approaches is damage diagnostics based on Bayesian inference, which leverages Bayesian techniques and physics-based modeling to address the inverse problem by aligning physics-based predictions with sensor monitoring observations [12]. In the past several years, numerous approaches have been developed using Bayesian methods for damage diagnostics of inland waterway infrastructure, such as miter gates. For instance, Ramancha *et al.*compared the finite element model with

[1]Corresponding Author.
Version 1.18, April 18, 2025

a surrogate model for Bayesian inference-based damage diagnostics of miter gate structural systems [13]. Levine *et al.*investigated the application of a Bayesian model updating technique in the diagnostics of miter gate anchorages and studied its implication on the design of such structures [14]. Vega *et al.*introduced a hybrid damage prognosis framework using the Bayesian method for miter gate components in navigational locks by minimizing human errors in evaluations and integrating abstract inspection data with data from SHM systems [4]. Qian *et al.* outlined a framework that combines machine learning with simulation updates for pitting corrosion detection in large infrastructures, utilizing an approximate Bayesian computation method to enhance model accuracy for future prognostics, demonstrated its efficacy on miter gates [15]. In another study, Qian *et al.* proposed a conditional invertible neural network-based Bayesian model updating method to enhance physics-based multi-scale corrosion simulations for large civil structures like miter gates. These simulations are crucial for predicting pitting corrosion and are integral to risk-based asset health management strategies [16].

Although Bayesian inference is a powerful technique for damage diagnostics in SHM, leveraging both physics-based simulations and sensor data, its effectiveness can be compromised by the quality and/or scarcity of monitoring data for a miter gate of interest [17]. This limitation is caused by the limited data sources available for SHM. Additionally, the accuracy of Bayesian inference-based diagnostics heavily relies on the fidelity of the simulation model. Various sources of uncertainty in the physics-based simulation—stemming from model simplifications, assumptions, or an incomplete understanding of the underlying physics—can lead to biased estimations of the structural damage state. On the other hand, numerous similar, yet different, miter gates have been inspected in the past, generating valuable inspection and monitoring data. Leveraging knowledge from these "nominal classes" of miter gates could provide an alternative approach to overcoming these limitations. This concept, known as population-based SHM, involves using knowledge from groups of similar structures to estimate the damage condition of a given structure. For a thorough discussion on various aspects of population-based SHM, see the trio of references from the University of Sheffield [18–20]. Among the numerous techniques available, one widely adopted method for leveraging data from different assets to diagnose the damage of a specific asset is domain adaptation or translation within the context of transfer learning. [21,22]. Domain adaptation is a technique where a model developed for a specific domain (the source domain) is adapted to work in a different but related domain (the target domain). This approach is particularly useful when the target domain has limited or no labeled data (such as the unknown damage state of a miter gate of interest). It involves adjusting the model so it can effectively transfer knowledge from one domain to another despite differences in data distribution [23].

In recent years, domain adaptation has increasingly been applied to the field of damage diagnostics. For example, Chun *et al.* introduced a self-training framework for unsupervised domain adaptation in concrete wall crack segmentation [24]. Chen *et al.* proposed a structural damage detection method that enhances detection performance by integrating one-dimensional and two-dimensional deep convolutional neural networks (CNN) for detailed spatiotemporal feature extraction from vibration data [25]. Huang *et al.* proposed a method that involves a Bayesian deep dual network that utilizes domain adaptation to transfer diagnostic insights from experimental setups to real-world machines with varying configurations and operational conditions [26]. Li *et al.* introduced a method using a deep convolutional neural network (DCNN) combined with Bayesian optimization and adaptive batch normalization (AdaBN) for predicting the remaining useful life of mechanical equipment [27]. Recently, adversarial-based domain adaptation includes methods like Generative Adversarial Networks (GANs), have gained popularity for their ability to create robust feature representations consistent across various domains. This characteristic makes GANs highly effective for domain adaptation challenges. Kwak et al. presented a diagnostic design solution that integrates Designable Data Augmentation (DDA) with Designable GAN and Prognosis and Health Management (PHM) technology, incorporating domain adaptation. This approach utilizes Bayesian transfer learning to transfer diagnostic knowledge from an established system to a new target system [28]. Despite the significant potential of domain adaptation in damage diagnostics, it also has its drawbacks, such as the risk of negative transfer. Additionally, it fails to leverage the rich information contained in physics-based simulations of a specific miter gate regarding the relationship between damage state and system response. Principled uncertainty quantification of the damage estimation is also challenging for such purely data-driven approaches.

Given that both physics-based Bayesian inference and domain adaptation in damage diagnostics have their own advantages and disadvantages, and their strengths and weaknesses complement each other, it is beneficial to determine when to use each method and how to integrate them for optimal damage state estimation. To this end, this paper proposes a novel Bayesian inference-based damage diagnostics approach Enhanced through Domain Translation (BiEDT), aiming to make more informed decisions regarding the damage state of a miter gate. The proposed method generally consists of three phases: The first phase converts observations from both the target and source miter gates into a common domain through domain translation; the second phase constructs a probabilistic model to determine the damage state of the target miter gate, using observations from the translated domain with known damage states of the source miter gates; finally, the method combines the results from the earlier phases with physics-based Bayesian inference through Bayesian model averaging. The main contributions of this paper can be summarized as follows:

- First, this study presents a novel framework that seamlessly integrates domain translation of observations with Bayesian inference techniques for damage diagnostics.
- Second, this paper synthesizes domain translation techniques with a conditional invertible neural network for the first time to enable damage diagnostics with quantified uncertainty.
- Third, a comparison of domain translation using Cycle-Consistent GAN (CycleGAN) and Domain-Adversarial Neural Network (DANN) in the proposed framework.
- Fourth, this paper proposes a Bayesian model averaging and selection method to synthesize different probabilistic estimates of the damage state.
- Finally, the proposed frameworks are demonstrated and compared using a practical application example of miter gate structural systems.

It is worth noting that the novelty of this paper lies in its comprehensive and innovative framework that seamlessly integrates domain translation techniques with Bayesian inference for damage diagnostics in miter gates. This holistic approach results in a robust and well-informed decision-making process concerning the damage state of miter gates, marking a significant advancement in the field of SHM.

The remainder of this paper is structured as follows: Sec. 2 provides a detailed background overview including Bayesian inference for probabilistic damage detection, health monitoring of miter gates, data augmentation with GANs in Bayesian models, and limitations of the existing methods. Sec. 3 formulates the problem and presents details of the proposed method. Sec. 4 uses a miter gate application example to demonstrate the proposed method. Finally, Sec. 5 presents the conclusion remarks of this paper.

2 Background

2.1 Probabilistic damage detection using Bayesian inference. In Bayesian inference-based probabilistic damage detection,

the observation data from a physical system are utilized to update its simulation model and estimate the structural damage characterized by uncertain model parameters $\boldsymbol{\theta}$. Let $\mathbf{y}_k = g(\mathbf{u}_{1:k}, \boldsymbol{\theta})$ be the concerned simulation model, where $\mathbf{y}_k \in \mathbb{R}^{N_y \times 1}$ are the model outputs at the kth time step, N_y is the number of model outputs, $\mathbf{u}_{1:k} \in \mathbb{R}^{(N_u \times k)\times 1}$ are the model inputs at the past k time steps, and N_u is the number of model inputs. The mathematical relation between the model prediction $\mathbf{y}_k$ and the observation data $\mathbf{y}_{o,k}$ can be expressed as follows [29]

$$\begin{aligned} \mathbf{y}_{o,k} &= g(\mathbf{u}_{1:k}, \boldsymbol{\theta}) + \delta(\mathbf{u}_{1:k}) + \boldsymbol{\varepsilon}_k, \\ &= \mathbf{y}_k + \delta(\mathbf{u}_{1:k}) + \boldsymbol{\varepsilon}_k, \end{aligned} \tag{1}$$

where $\delta(\mathbf{u}_{1:k})$ is the model discrepancy term, $\boldsymbol{\varepsilon}_k \sim N(\mathbf{0}, \boldsymbol{\Sigma}_k)$ is the Gaussian noise term with zero mean and the following covariance matrix:

$$\boldsymbol{\Sigma}_k = \begin{pmatrix} \sigma_1^2 & 0 & \cdots & 0 \\ 0 & \sigma_2^2 & \cdots & 0 \\ \vdots & \vdots & \ddots & \vdots \\ 0 & 0 & \cdots & \sigma_{N_y}^2 \end{pmatrix} \in \mathbb{R}^{N_y \times N_y}. \tag{2}$$

Given the observations of the input and output, the joint posterior distribution of the uncertainty parameters $\boldsymbol{\theta}$ can be obtained by applying Bayes' rule as

$$f(\boldsymbol{\theta}|\mathbf{u}_{1:k}, \mathbf{y}_{o,1:k}) = \frac{L(\mathbf{y}_{o,1:k}|\mathbf{u}_{1:k}, \boldsymbol{\theta}) f(\boldsymbol{\theta})}{\int L(\mathbf{y}_{o,1:k}|\mathbf{u}_{1:k}, \boldsymbol{\theta}) f(\boldsymbol{\theta}) d\boldsymbol{\theta}}, \tag{3}$$

where $f(\boldsymbol{\theta})$ and $f(\boldsymbol{\theta}|\mathbf{u}_{1:k}, \mathbf{y}_{o,1:k})$ are the prior and posterior distributions of $\boldsymbol{\theta}$, respectively, and $L(\mathbf{y}_{o,1:k}|\mathbf{u}_{1:k}, \boldsymbol{\theta})$ is the likelihood function, which measures the agreement between the model prediction $\mathbf{y}_k$ and the observation value $\mathbf{y}_{o,k}$.

2.2 Structural health monitoring of miter gates in inland waterway networks. In the United States, the USACE maintains and operates 236 miter gate structures, as shown in Fig. 1, at 191 sites. These miter gates constitute a network that plays a crucial role in the inland waterway transportation system. More than half of these structures have been beyond their 50-year expected service life. Maintenance and upkeep plans are critical for the optimal operation of these miter gates, as unexpected closures can prevent shippers from completing their scheduled transportation tasks, leading to unpredictable economic losses.

Fig. 1 Miter gates in inland waterway navigation

One of the most common damage modes in miter gate structure is a gap that arises from the loss of contact between the gate quoin block and the wall quoin block the bottom of the gate, as shown in Fig. 2. This gap will further lead to the stress redistribution in the gate structure stress, forming a high stress zone, which may exceed the acceptable limit state and lead to failure. Because such gaps are often underwater, they cannot be directly observed. Instead, one can infer the gaps from the measurement data collected by the sensor installed in the high stress zone.

Fig. 2 Illustration of "gap" on miter gate structures

2.3 Augmenting observation data in Bayesian inference using Generative Adversarial Networks (GANs). In Bayesian model updating, the observation data is of paramount importance as it provides insightful information for estimating model parameters and quantifying uncertainty. Thus, the accuracy and effectiveness of Bayesian model updating highly depend on both the quality and quantity of sensor-monitoring data. However, the available data in practical engineering is often limited, which seriously hinders the effectiveness of Bayesian model updating. To overcome this limitation, in our previous work, we applied a data augmentation technique, which generates synthetic data through the process of sampling and transformation of existing data to increase the diversity and volume of an existing dataset, and thereby improving the effectiveness of the Bayesian model updating-based damage detection. This data augmentation technique has been demonstrated in our previous work in Refs. [17,30].

Fig. 3 provides an overview of our previous approach using a technique called CycleGAN to enhance Bayesian inference for estimating the damage status (i.e., gap length) of miter gates. Assuming the two miter gates share operational and environmental similarities but not identical conditions, we employed CycleGAN to enrich the dataset of "Miter gate 2" by translating sensor data from "Miter gate 1", thus increasing the confidence of Bayesian inference-based damage estimation (i.e., gap length) of "Miter gate 2". The whole technical route consists of four parts: (1) data preprocessing, (2) synthetic data generation, (3) accuracy verification of synthetically generated data, and (4) augmenting Bayesian Inference with synthetic data.

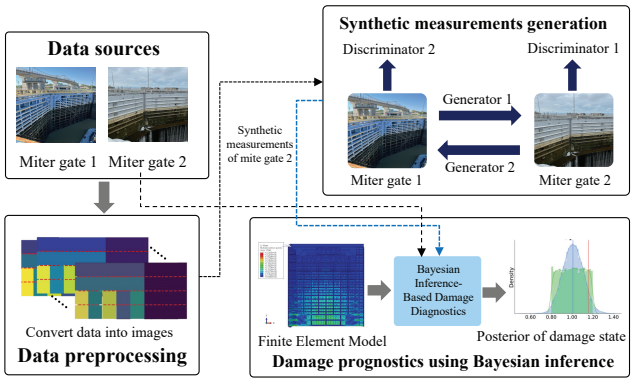

Fig. 3 A framework proposed in our previous research [17,30]

2.4 Limitations of existing methods. While the results of our previous research have shown the promise of data augmentation in enhancing the performance of Bayesian inference-based damage diagnostics, it also has several limitations. *First*, the method pre-

sented in Refs. [17,30] and as shown in Fig. 3 assumes that the damage states of the two miter gates of interest remain unchanged for the time duration of data collection. This assumption greatly limits the application of the method since the damage states of the inspected miter gates are different most of the time. *Second*, the trained inference model only applies to one unknown damage state due to the first limitation. It needs to be retrained whenever the damage state of the miter gate of interest changes. *Third*, the method presented in Refs. [17,30] mainly focuses on augmenting the observation data, which will subsequently be used in Bayesian inference using physics-based simulations. The damage estimation in this case highly dependent on the fidelity of the simulation model. It, therefore, cannot overcome the aforementioned limitations of Bayesian inference-based damage diagnostics caused by the imperfection of the physics-based simulations.

Motivated by overcoming the limitations of our previous method and developing a versatile approach for enhancing Bayesian inference-based damage diagnostics, in Sec. 3, we propose a novel framework called Bayesian inference-based damage diagnostics approach Enhanced through Domain Translation (BiEDT). Even though BiEDT is developed for miter gate applications, it is very generalized and applicable to other engineering systems.

3 Proposed Method

In this section, we first formulate the problem that we aim to solve. After that, we will present the proposed method in detail.

3.1 Problem formulation.

The objective of this paper is to estimate the damage state (i.e., gap) of a miter gate of interest based on three main data sources, namely (1) structural monitoring data of the miter gate itself, which has an unknown damage state; (2) monitoring data from similar, but different, miter gates whose damage states have already been inspected; and (3) a physics-based computational simulation model of the miter gate of interest.

For the sake of explanation, we refer to the miter gate of interest, which has an unknown damage state, as the *target miter gate*. Similarly, we refer to the miter gates whose damage states have already been inspected as *source miter gates*. This terminology is analogous to definitions commonly used in transfer learning within the machine learning community. We define the following variables to represent the data sources and models.

- $\mathbf{y}_{o,\text{tg},i} \in \mathbb{R}^{N_t \times N_s}, \forall i = 1, \cdots, N_{ot}$: the i-th group of monitoring data of the target miter gate over N_t time steps from N_s strain gauges on the gate, where N_{ot} is the total number of available monitoring datasets.
- $\mathbf{y}_{o,\text{sr},i} \in \mathbb{R}^{N_t \times N_s}, \forall i = 1, \cdots, N_{os}$: the i-th group of monitoring data of the source miter gates over N_t time steps from N_s strain gauges on the gates, where N_{os} is the total number of available monitoring datasets. Note that here the value of N_{os} could be different from that of N_{ot}, and the N_{os} datasets could come from different source miter gates.
- $\boldsymbol{\theta}_{\text{sr},i}, i = 1, \cdots, N_{os}$: inspected damage state $\boldsymbol{\theta}_{\text{sr}}$ of the source miter gates corresponding to the i-th group of monitoring data $\mathbf{y}_{o,\text{sr},i}$ of the source miter gates.
- $\boldsymbol{\theta}_{\text{tg},i}, i = 1, \cdots, N_{ot}$: unknown damage state $\boldsymbol{\theta}_{\text{tg}}$ of the target miter gate corresponding to the i-th group of monitoring data $\mathbf{y}_{o,\text{tg},i}$.
- $\mathbf{y}_{\text{tg}} = G(\boldsymbol{\theta}, \mathbf{u})$: computational simulation model (i.e., finite element analysis model) of the target miter gate, which can predict the strain response for given damage state $\boldsymbol{\theta}$ and load condition $\mathbf{u}$ (i.e., water level for the miter gate case).

It is worth mentioning that even though $\{\boldsymbol{\theta}_{\text{tg},i}, i = 1, \cdots, N_{ot}\}$ and $\{\boldsymbol{\theta}_{\text{sr},i}, i = 1, \cdots, N_{os}\}$ represent the damage states of different miter gates, they are domain-invariant quantities. For instance, all the gap lengths of the miter gates in the case study of this paper are bounded between 0 to 130 inches. Based on the above definitions, the problem that needs to be solved is to find the following posterior distribution of the unknown damage state, $\boldsymbol{\theta}_{\text{tg},i}$,

$$f(\boldsymbol{\theta}_{\text{tg},i} | (\tilde{\mathbf{y}}_{o,\text{sr}}, \tilde{\boldsymbol{\theta}}_{\text{sr}}, \mathbf{y}_{o,\text{tg},i}; \mathbb{G})), \ \forall i = 1, \cdots, N_{ot}, \tag{4}$$

where $\tilde{\mathbf{y}}_{o,\text{sr}} \doteq \{\mathbf{y}_{o,\text{sr},i}, i = 1, \cdots, N_{os}\}$, $\tilde{\boldsymbol{\theta}}_{\text{sr}} \doteq \{\boldsymbol{\theta}_{\text{sr},i}, i = 1, \cdots, N_{os}\}$, and $\mathbb{G}$ represents the simulation model $\mathbf{y}_{\text{tg}} = G(\boldsymbol{\theta}, \mathbf{u})$.

If we only have monitoring data from the target miter gate, the posterior distribution $f(\boldsymbol{\theta}_{\text{tg},i} | (\mathbf{y}_{o,\text{tg},i}; \mathbb{G}))$ can be solved using conventional Bayesian model updating methods [13,31]. However, the limited monitoring data $\mathbf{y}_{o,\text{tg},i}$ from the target gate and various uncertainty sources in the simulation model, $\mathbf{y}_{\text{tg}} = G(\boldsymbol{\theta}, \mathbf{u})$, could result in large uncertainty or bias in the estimated damage state $\boldsymbol{\theta}_{\text{tg},i}$. Although damage inspection and monitoring data, $\{\boldsymbol{\theta}_{\text{sr},i}, \mathbf{y}_{o,\text{sr},i}\}, i = 1, \cdots, N_{os}$, from similar but different miter gates (referred to as source miter gates) can potentially mitigate the impact of limited monitoring data of the target gate and model uncertainty of $\mathbf{y}_{\text{tg}} = G(\boldsymbol{\theta}, \mathbf{u})$ on damage state estimation, effectively leveraging these data sources for Bayesian damage estimation of a target miter gate (i.e., solving Eq. (4)) remains a formidable challenge. This challenge is mainly caused by the disconnect between the damage state, $\boldsymbol{\theta}_{\text{tg},i}$, of the target miter gate and the monitoring and inspection data (i.e., $\tilde{\mathbf{y}}_{o,\text{sr}}$) of similar, yet different, miter gates. Motivated by overcoming this challenge, in this paper, we propose a novel framework called BiEDT that integrates domain adaptation/translation techniques with Bayesian inference-based damage diagnostics. In the subsequent sections, we will present the proposed BiEDT framework in detail.

3.2 Overview of the proposed BiEDT framework.

Figure 4 provides an overview of the proposed method. The basic idea is to leverage the inspection and monitoring data from similar, yet different, miter gates to develop an alternative method for estimating the damage state of the target miter gate. This method will complement the commonly employed Bayesian model updating technique, which relies on computational simulation models (see descriptions in Sec. 2.1). Once the alternative estimation method is established, we will integrate the damage state estimations from various approaches using a Bayesian framework.

More specifically, in order to overcome the challenge that $\boldsymbol{\theta}_{\text{tg},i}$ and $\tilde{\mathbf{y}}_{o,\text{sr}}$ are disconnected, we first employ domain translation techniques to translate measurements of the source and target miter gates into the same analysis domain as follows

$$\begin{aligned} \boldsymbol{\eta}_{o,\text{tg},i} &= \varphi(\mathbf{y}_{o,\text{tg},i}), \ i = 1, \cdots, N_{ot}, \\ \boldsymbol{\eta}_{o,\text{sr},i} &= \varphi(\mathbf{y}_{o,\text{sr},i}), \ i = 1, \cdots, N_{os}, \end{aligned} \tag{5}$$

where $\boldsymbol{\eta}_{o,\text{tg},i}, \boldsymbol{\eta}_{o,\text{sr},i} \in \Omega_\eta$, which is a domain common to both the source and target miter gates, and $\varphi(\cdot)$ is a domain translator which translates measurements from one domain to a domain of interest. As detailed in Sec. 3.3, two types of domain translation/adaptation approaches will be investigated to achieve the purpose of measurement translation.

Since there is a unknown nonlinear relationship between $\{\boldsymbol{\theta}_{\text{sr},i}, i = 1, \cdots, N_{os}\}$ and $\{\boldsymbol{\eta}_{o,\text{sr},i}, i = 1, \cdots, N_{os}\}$, the same unknown relationship also exists between $\boldsymbol{\theta}_{\text{tg},i}$ and $\boldsymbol{\eta}_{o,\text{tg},i}$ in the translated domain, Ω_η. Given that $\boldsymbol{\eta}_{o,\text{sr},i} \in \Omega_\eta$ and $\boldsymbol{\eta}_{o,\text{tg},i} \in \Omega_\eta$ are in the same domain, we, therefore, can build a model to learn the unknown nonlinear relationship between the damage state $\boldsymbol{\theta}$ and the translated observations $\boldsymbol{\eta}$ of the miter gates using data $\{\boldsymbol{\theta}_{\text{sr},i}, i = 1, \cdots, N_{os}\}$ and $\{\boldsymbol{\eta}_{o,\text{sr},i}, i = 1, \cdots, N_{os}\}$ as follows

$$\boldsymbol{\theta} = H(\boldsymbol{\eta}; (\tilde{\boldsymbol{\eta}}_{o,\text{sr}}, \tilde{\boldsymbol{\theta}}_{\text{sr}})), \tag{6}$$

where $H(\cdot)$ is a probabilistic function that maps $\boldsymbol{\eta}$ to $\boldsymbol{\theta}$, which is trained using data of $\{\tilde{\boldsymbol{\eta}}_{o,\text{sr}}, \tilde{\boldsymbol{\theta}}_{\text{sr}}\}$, and $\tilde{\boldsymbol{\eta}}_{o,\text{sr}} \doteq \{\boldsymbol{\eta}_{o,\text{sr},i}, i =$

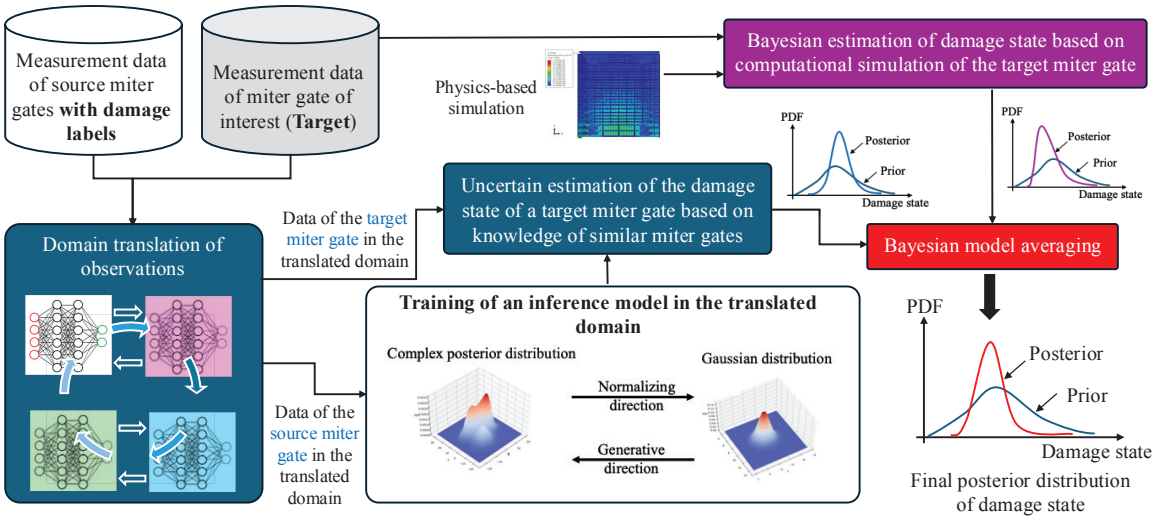

Fig. 4 Overview of the proposed BiEDT framework

$1, \cdots, N_{OS}\}$. In this paper, a conditional invertible neural network is employed to build such a model for the mapping. More details are provided in Sec. 3.4.

By using the translated measurements of the target miter gate and the model learned in Eq. (6), we can then estimate the damage state of the target miter gate as

$$\hat{\boldsymbol{\theta}}_{\text{tg},i} = H(\boldsymbol{\eta}_{o,\text{tg},i}; (\tilde{\boldsymbol{\eta}}_{o,\text{sr}}, \tilde{\boldsymbol{\theta}}_{\text{sr}})), \tag{7}$$

where $\boldsymbol{\eta}_{o,\text{tg},i} = \varphi(\mathbf{y}_{o,\text{tg},i})$ as given in Eq. (5).

Until now, we established an approach to probabilistically estimate the damage state of the target miter gate by leveraging inspection and monitoring data of source miter gates. This proposed approach integrates domain translation techniques with probabilistic damage diagnostics to fill the gap between two types of similar but different miter gates. In addition to this new way of estimating the damage state, as mentioned above, we also have another way of estimating the damage state of the target miter gate by using the physics-based computational simulation model (i.e., $\mathbf{y}_{\text{tg}} = G(\boldsymbol{\theta}, \mathbf{u})$) of the target miter gate. Using Bayesian method, the damage state can be estimated using only the measurements of the target miter gate as

$$f(\boldsymbol{\theta}_{\text{tg},i}|(\mathbf{y}_{o,\text{tg},i}; \mathbb{G})) \propto L(\mathbf{y}_{o,\text{tg},i}|(\boldsymbol{\theta}_{\text{tg},i}; \mathbb{G}))\, f_{\boldsymbol{\theta}}(\boldsymbol{\theta}_{\text{tg},i}), \tag{8}$$

where $L(\mathbf{y}_{o,\text{tg},i}|(\boldsymbol{\theta}_{\text{tg},i}; \mathbb{G}))$ is a likelihood function and $f_{\boldsymbol{\theta}}(\boldsymbol{\theta}_{\text{tg},i})$ is the prior distribution of the damage state of the target miter gate.

Both Eqs. (7) and (8) can provide an estimation of the damage state of the target gate using different approaches. The next question that needs to be answered now is how to combine these two types of estimations together to get a final estimated posterior distribution of the damage state. An intuitive combination of these two types of estimations is to use the estimation given in Eq. (7) as the prior distribution of Eq. (8). Such an approach, however, risks double-counting the measurement data of the target miter gate in the Bayesian damage diagnostics, as both Eqs. (7) and (8) use $\mathbf{y}_{o,\text{tg},i}$ as inputs, despite Eq. (7) only employing the translated information from $\mathbf{y}_{o,\text{tg},i}$.

To mitigate the risk of using the same information twice, a Bayesian model averaging approach is developed by combining estimations from the two different types of approaches (as illustrated in Fig. 4) [32]. The posterior distribution given in Eq. (4) is thus approximated as

$$\begin{aligned} &f(\boldsymbol{\theta}_{\text{tg},i}|(\tilde{\mathbf{y}}_{o,\text{sr}}, \tilde{\boldsymbol{\theta}}_{\text{sr}}, \mathbf{y}_{o,\text{tg},i}; \mathbb{G})) \\ &\approx f_{DT}(\boldsymbol{\theta}_{\text{tg},i}) p(\mathbb{H}|\mathbf{D}) + f(\boldsymbol{\theta}_{\text{tg},i}|(\mathbf{y}_{o,\text{tg},i}; \mathbb{G})) p(\mathbb{G}|\mathbf{D}), \end{aligned} \tag{9}$$

where $f_{DT}(\boldsymbol{\theta}_{\text{tg},i})$ represents the posterior distribution obtained from domain translation (i.e., Eq. (6)), $\mathbb{H}$ represents the overall domain translation model for estimating the damage state of the target miter gate, $\mathbf{D} \doteq \{\tilde{\mathbf{y}}_{o,\text{sr}}, \tilde{\boldsymbol{\theta}}_{\text{sr}}, \mathbf{y}_{o,\text{tg},i}\}$, and $p(\mathbb{H}|\mathbf{D})$ and $p(\mathbb{G}|\mathbf{D})$ represent respectively the weights of different approaches or models in the model averaging. In addition to the above model averaging, we can also select which model or poster distribution to use in decision-making through Bayesian hypothesis testing. More details of such a Bayesian model averaging or model selection are presented in Sec. 3.5.

In summary, as shown in Fig. 4, the proposed framework consists of three main modules:

(1) *Domain translation of observations*: This module concentrates on translating observations of both the target gate and the source gates into a common domain. This translation is essential for building a connection between the damage state of the target miter gate and the inspection and measurements of the source miter gates.
(2) *Bayesian inference-based damage diagnostics in the translated domain*: This module focuses on building a model for inferring the damage state of the target miter gate based on observation data with labeled damage states of the source miter gates in the translated domain.
(3) *Bayesian model averaging for the integration of probabilistic estimations*: Building upon results and models from the previous two modules, as illustrated in Fig. 4, this module combines both posterior distribution from computational simulation (i.e., Eq. (7)) and inference results in translated domain (i.e., Eq. (8)) by solving Eq. (9), thereby obtain the final posterior distribution of the damage state of the target miter gate.

In the following subsections, we explain each of the above modules in detail.

3.3 Domain translation of observations. In this paper, two types of domain-translation approaches are investigated to perform domain translation of miter gate observations. The two approaches, namely the CycleGAN-based method and Domain-Adversarial Neural Network (DANN)-based method, translate observations of a target miter gate to different domains. In particular, the CycleGAN-based method translates observations of the target miter gate directly into observations of source miter gates while the DANN-based method translates observations of both the target and source miter gates into a common/shared domain that is different from the original domains of both types of miter gates. In what

follows, we explain the main idea of the studied two approaches in detail.

3.3.1 CycleGAN-based domain translation. CycleGAN is a method introduced by Zhu *et al.*for addressing unpaired image-to-image translation challenges [33]. It facilitates the transformation of images from one style into another, for example, converting images of horses into zebras or summer scenes into winter [34]. It is an effective technique for discovering and learning the relationships between different unpaired domains.

Fig. 5 illustrates the architecture of CycleGAN as it is applied to domain translation for miter gates. The architecture consists of two main components: two generator networks and two discriminator networks. Each generator-discriminator pair is responsible for one direction of image translation between two distinct domains, Domain A (source miter gate) and Domain B (target miter gate). The first generator, $\mathbb{K}(\cdot)$, translates images from Domain A to Domain B, while the second generator, $\mathbb{F}(\cdot)$, performs the inverse, translating images from Domain B to Domain A. Correspondingly, each discriminator, $\mathbb{D}_1(\cdot)$ and $\mathbb{D}_2(\cdot)$, aims to distinguish between the translated images and real images in their respective domains. A novel and critical aspect of CycleGAN is its use of a cycle consistency loss. This loss function ensures that an image from one domain can be translated to the other domain and then back again to the original domain, with the goal of retaining the original image's content and structure [33]. Mathematically, for an image $\mathcal{X}$ from Domain A, the cycle consistency loss ensures that $\mathbb{F}(\mathbb{K}(\mathcal{X})) \approx \mathcal{X}$, and similarly, for an image $\mathcal{Y}$ from Domain B, it ensures that $\mathbb{K}(\mathbb{F}(\mathcal{Y})) \approx \mathcal{Y}$. Next, we will delve into each component of the CycleGAN and provide detailed explanations.

CycleGAN in our study utilizes a modified U-Net architecture for its generators $\mathbb{K}(\cdot)$ and $\mathbb{F}(\cdot)$. The U-Net architecture is particularly effective due to its encoder-decoder structure with skip connections that help preserve fine-grained details throughout the network:

- *Encoder*: The encoder part typically consists of convolutional layers that successively downsample the input image, capturing increasingly abstract representations of the input.
- *Decoder*: The decoder uses transposed convolutions (or upsampling layers followed by convolutions) to progressively upsample the encoded representations back to the original image size. The upsampling process reintegrates finer details into the synthesized image.
- *Skip Connections*: These connections pass information directly from the encoder to the corresponding layers in the decoder, helping in recovering fine details that might be lost during downsampling.

This architecture allows CycleGAN's generators to efficiently translate the input image from one domain to the other while maintaining critical information. The discriminators in CycleGAN, often referred to as PatchGAN, classify whether small patches of the image are real or fake. This approach differs from traditional full-image discriminators by focusing on the realism of local image patches [33]. PatchGAN consists of a few convolutional layers that downsample the image to a smaller set of patches. Each patch in the output map is independently classified as real or fake, and the discriminator's final output is the average of these classifications. This method is computationally less intensive and focuses on getting high-frequency details right, which is often enough to make the whole image appear convincingly real or accurately translated.

The loss functions in CycleGAN play a crucial role in enabling the effective translation of images between two unpaired domains. Adversarial losses, cycle consistency loss, and identity loss are components in the loss function of CycleGAN. The first part of the adversarial losses is shown as follows [34]

$$\begin{aligned}\mathcal{L}_{\text{GAN}}\left(\mathbb{K},\mathbb{D}_1,X,Y\right) = \mathbb{E}_{\mathcal{Y}\sim p_{\text{data}}\left(\mathcal{Y}\right)}\left[\log \mathbb{D}_1(\mathcal{Y})\right] \\ + \mathbb{E}_{\mathcal{X}\sim p_{\text{data}}\left(\mathcal{X}\right)}\left[\log\left(1-\mathbb{D}_1(\mathbb{K}(\mathcal{X}))\right)\right],\end{aligned} \tag{10}$$

where the image input for domain A and B are $X = \{\mathcal{X}_1, \cdots, \mathcal{X}_N\}$, $Y = \{\mathcal{Y}_1, \cdots, \mathcal{Y}_N\}$ respectively. $\mathbb{K}(\cdot)$ is the generator that generates synthetic data for domain B. $\mathbb{D}_1(\cdot)$ is the discriminator that distinguishes between translated samples $\hat{\mathcal{Y}}_j = \mathbb{K}(\mathcal{X}_j)$ and real sample $\mathcal{Y}_j$. The data distributions are denoted as $\mathcal{X} \sim p_{\text{data}}(\mathcal{X})$ and $\mathcal{Y} \sim p_{\text{data}}(\mathcal{Y})$.

Another adversarial loss function is given as [34]

$$\begin{aligned}\mathcal{L}_{\text{GAN}}\left(\mathbb{F},\mathbb{D}_2,Y,X\right) = \mathbb{E}_{\mathcal{X}\sim p_{\text{data}}\left(\mathcal{X}\right)}\left[\log \mathbb{D}_2(\mathcal{X})\right] \\ + \mathbb{E}_{\mathcal{Y}\sim p_{\text{data}}\left(\mathcal{Y}\right)}\left[\log\left(1-\mathbb{D}_2(\mathbb{F}(\mathcal{Y}))\right)\right]\end{aligned}, \tag{11}$$

where $\mathbb{F}(\cdot)$ is the generator that generates synthetic data for domain A. $\mathbb{D}_2(\cdot)$ is the discriminator that distinguishes between translated samples $\hat{\mathcal{X}}_j = \mathbb{F}(\mathcal{Y}_j)$ and real sample $\mathcal{X}_j$.

The cycle consistency loss is given as [34]

$$\begin{aligned}\mathcal{L}_{\text{cyc}}(\mathbb{K},\mathbb{F}) = \mathbb{E}_{\mathcal{X}\sim p_{\text{data}}\left(\mathcal{X}\right)}\left[\|\mathbb{F}(\mathbb{K}(\mathcal{X}))-\mathcal{X}\|_1\right] \\ + \mathbb{E}_{\mathcal{Y}\sim p_{\text{data}}\left(\mathcal{Y}\right)}\left[\|\mathbb{K}(\mathbb{F}(\mathcal{Y}))-\mathcal{Y}\|_1\right]\end{aligned}, \tag{12}$$

where $\|\cdot\|_1$ denotes the L1 norm, which penalizes the absolute differences between the original and reconstructed images.

The identity mapping loss is given by [34]

$$\mathcal{L}_{\text{id}}(\mathbb{K},\mathbb{F}) = \|\mathbb{K}(\mathcal{Y})-\mathcal{Y}\|_1 + \|\mathbb{F}(\mathcal{X})-\mathcal{X}\|_1. \tag{13}$$

Thus, the overall loss function of CycleGAN is denoted as

$$\begin{aligned}\mathcal{L}(\mathbb{K},\mathbb{F},\mathbb{D}_1,\mathbb{D}_2) = \mathcal{L}_{\text{GAN}}\left(\mathbb{K},\mathbb{D}_1,X,Y\right) \\ + \mathcal{L}_{\text{GAN}}\left(\mathbb{F},\mathbb{D}_2,Y,X\right), \\ + \mathcal{L}_{\text{cyc}}(\mathbb{K},\mathbb{F}) + \mathcal{L}_{\text{id}}(\mathbb{K},\mathbb{F}),\end{aligned} \tag{14}$$

and we aim to solve

$$\mathbb{K}^*,\mathbb{F}^* = \arg\min_{\mathbb{F},\mathbb{K}}\max_{\mathbb{D}_1,\mathbb{D}_2}\mathcal{L}\left(\mathbb{K},\mathbb{F},\mathbb{D}_1,\mathbb{D}_2\right). \tag{15}$$

For the training of the CycleGAN model in this paper, we have $X \doteq \{\mathbf{y}_{o,\text{tg},i}, \forall i = 1,\cdots,N_{ot}\}$ and $Y \doteq \{\mathbf{y}_{o,\text{sr},i}, \forall i = 1,\cdots,N_{os}\}$. After the training of the CycleGAN model, we can translate observations of the target miter gate into their counterparts of the source miter gates as

$$\hat{\mathbf{y}}_{o,\text{tg2sr},i} \approx \mathbb{F}(\mathbf{y}_{o,\text{tg},i}), \forall i = 1,\cdots,N_{ot}. \tag{16}$$

Additionally, we can obtain the reconstrcuted observations of the source miter gates through the CycleGAN model as

$$\hat{\mathbf{y}}_{o,\text{sr2sr},i} \approx \mathbb{F}(\mathbb{K}(\mathbf{y}_{o,\text{sr},i})), \forall i = 1,\cdots,N_{os}. \tag{17}$$

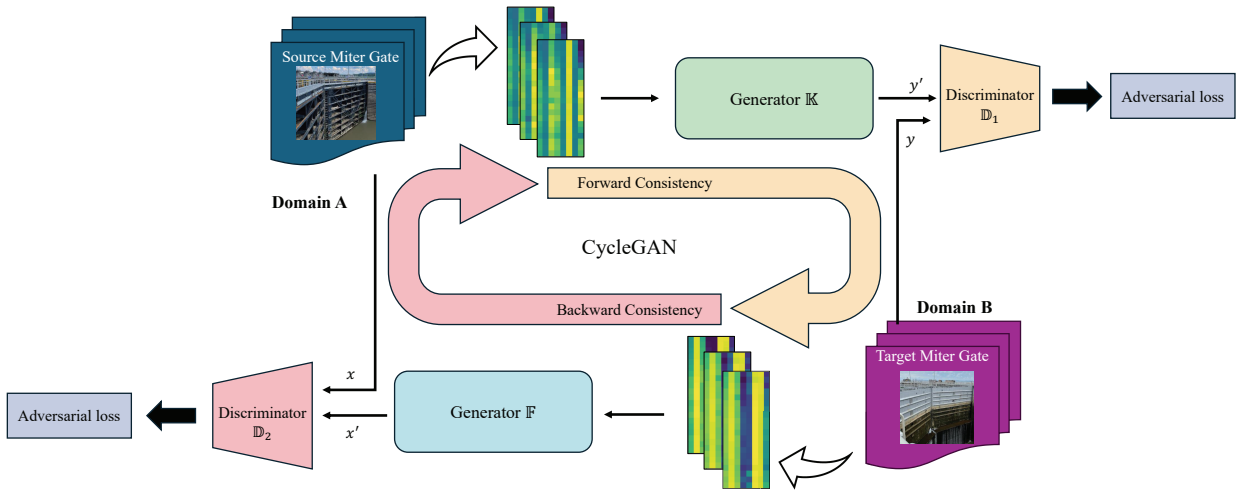

Fig. 5 The structure of CycleGAN for translation of miter gate observations.

3.3.2 Domain-Adversarial Neural Network (DANN) -based domain translation. The Domain-Adversarial Neural Network (DANN) introduces a representation learning method for domain adaptation, where training and testing data originate from similar yet different distributions [35]. This model is designed to work with labeled data from the source domain and unlabeled data from the target domain, eliminating the need for labeled target-domain data. Throughout training, DANN encourages the development of features that are both discriminative for the task at hand within the source domain and non-discriminative regarding the domain differences. This dual capability is facilitated by introducing a few standard layers and a gradient reversal layer, enabling training via standard backpropagation and stochastic gradient descent [35].

Fig. 6 illustrates the architecture of DANN for the application to domain translation of miter gates. DANN was originally developed primarily for classification tasks. However, when adapting DANN for a regression task instead, the structural modifications primarily involve the output layer and the loss functions used, while retaining the core adversarial architecture. Here's how the model is structured

- *Feature Extractor*: This is a neural network that processes input data to extract useful features. The architecture of this network includes multiple dense layers designed to capture the nuances necessary for predicting continuous values.
- *Domain Classifier*: This component tries to determine the domain of the input features (source vs. target) and is pivotal for ensuring that the features are domain-invariant. It typically consists of a few dense layers followed by a binary classification output that indicates the domain.
- *Gradient Reversal Layer (GRL)*: Positioned between the feature extractor and the domain classifier, the GRL is crucial for the adversarial training aspect of DANN. It reverses the gradient during backpropagation, effectively making the domain classifier's job harder, which in turn forces the feature extractor to produce more domain-invariant features.
- *Regressor*: A regressor is used at the output of the feature extractor for the primary task of regression. The activation function is linear.

DANN incorporates concepts from GANs to facilitate the development of features that are effective across different domains. This adversarial learning approach involves a two-player game: the first player is a domain classifier $\mathbb{G}_d(\cdot)$ tasked with differentiating between source and target domain data. In contrast, the second player is a feature extractor $\mathbb{G}_f(\cdot)$ that aims to generate features indistinguishable by $\mathbb{G}_d(\cdot)$, effectively confusing the discriminator by producing domain-invariant features.

The training of these components is adversarial. The feature extractor $\mathbb{G}_f(\cdot)$'s parameters $\boldsymbol{\theta}_f$ are optimized to maximize the discriminator $\mathbb{G}_d(\cdot)$'s loss, thereby fooling $\mathbb{G}_d(\cdot)$ into misclassifying the domain of the features. Conversely, the parameters $\boldsymbol{\theta}_d$ of $\mathbb{G}_d(\cdot)$ are trained to minimize its loss, improving its ability to classify the domain of the data correctly. Simultaneously, the loss of a label regressor $\mathbb{G}_r(\cdot)$, responsible for the source domain regression, is minimized. The regression loss is given as

$$\mathcal{L}_{\mathrm{r}} = \frac{1}{n_s} \sum_{i=1}^{n_s} |r_i - \mathbb{G}_r(\mathcal{X}_i)| \tag{18}$$

where n_s represents the sample size of the source domain data and r_i is the label/response of the source domain data.

The domain loss, $\mathcal{L}_{\mathrm{d}}$ is expressed as introduced in [35] by evaluating the difference between the domain label (0 for source and 1 for target domain) and the domain classifier output, $\mathbb{G}_d(\mathbb{G}_f(\mathcal{X}))$. Because there are no labels for target domain data in the training set, the total loss is given as

$$\mathcal{L}(\boldsymbol{\theta}_f, \boldsymbol{\theta}_r, \boldsymbol{\theta}_d) = \mathcal{L}_{\mathrm{r}} + \lambda \mathcal{L}_{\mathrm{d}}, \tag{19}$$

where λ is a weighting parameter that balances the contribution of the adversarial loss. And we intend to solve [35]

$$\begin{aligned} (\hat{\boldsymbol{\theta}}_f, \hat{\boldsymbol{\theta}}_r) &= \arg\min_{\theta_f, \theta_r} \mathcal{L}(\boldsymbol{\theta}_f, \boldsymbol{\theta}_r, \hat{\boldsymbol{\theta}}_d), \\ \hat{\boldsymbol{\theta}}_d &= \arg\max_{\theta_d} \mathcal{L}(\hat{\boldsymbol{\theta}}_f, \hat{\boldsymbol{\theta}}_y, \boldsymbol{\theta}_d). \end{aligned} \tag{20}$$

For the training of the DANN model in this paper, the data used include $\{\mathbf{y}_{o,\mathrm{tg},i}, \forall i = 1, \cdots, N_{ot}\}$, $\{\boldsymbol{\theta}_{\mathrm{sr},i}, i = 1, \cdots, N_{os}\}$, and $\{\mathbf{y}_{o,\mathrm{sr},i}, \forall i = 1, \cdots, N_{os}\}$. After the training of the DANN model, we have the common features of the observations of the target miter gate and the source miter gates as

$$\begin{aligned} \boldsymbol{\eta}_{\mathrm{DANN,tg},i} &\approx \varphi_{\mathrm{DANN}}(\mathbf{y}_{o,\mathrm{tg},i}),\ i = 1, \cdots, N_{ot}, \\ \boldsymbol{\eta}_{\mathrm{DANN,sr},i} &\approx \varphi_{\mathrm{DANN}}(\mathbf{y}_{o,\mathrm{sr},i}),\ i = 1, \cdots, N_{os}, \end{aligned} \tag{21}$$

where $\boldsymbol{\eta}_{\mathrm{DANN,tg},i}$ and $\boldsymbol{\eta}_{\mathrm{DANN,sr},i}$ are respectively the translated observations of the target and source miter gates, and $\varphi_{\mathrm{DANN}}(\cdot)$ represents the overall DANN model.

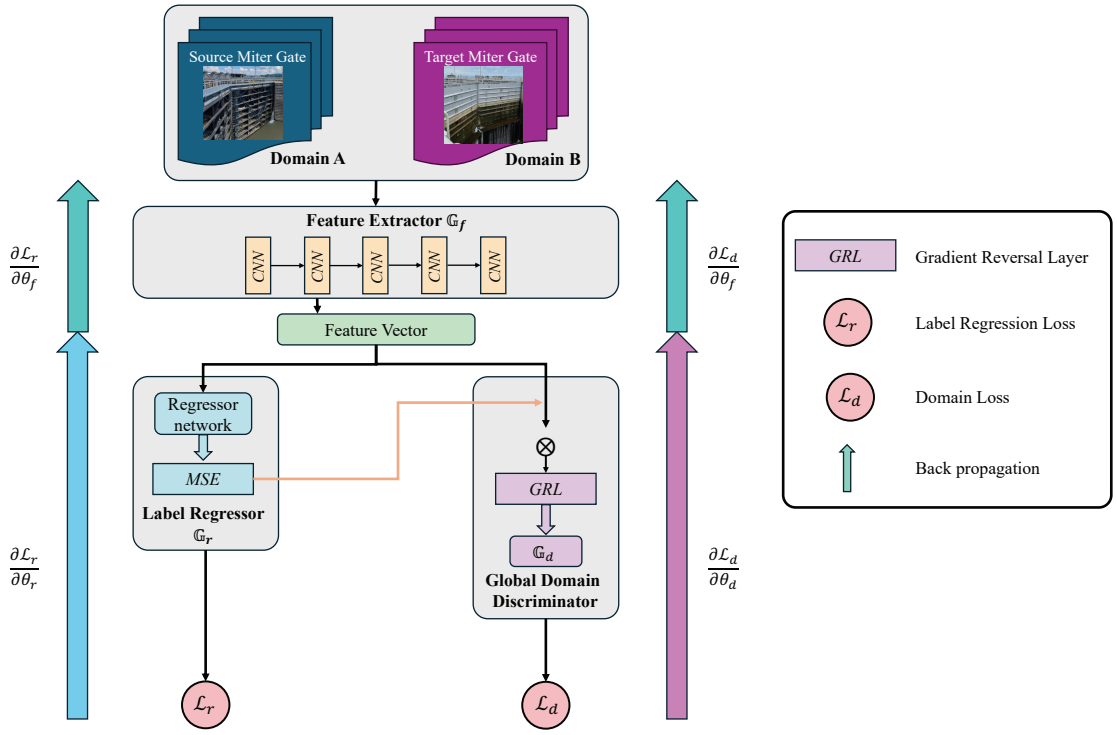

Fig. 6 The structure of DANN for translation of miter gate observations.

3.4 Bayesian inference-based damage diagnostics in the translated domain. Using the approaches described in Sec. 3.3, we can translate the observations of the source and target miter gates into a common domain. Based on the translated data from the source miter gates, in this section, we construct an inverse model to estimate the damage state of the target gate for given observations in the translated domain (i.e., Eqs. (6) and (7)). Given the complex nonlinear relationship between the damage state and the transformed observations, along with various sources of uncertainty in the domain translation, we employ a normalizing flow-based approach [36–38]. This method uses conditional invertiable neural networks (cINN) to construct the inverse model and perform Bayesian inference-based damage diagnostics of the target miter gate in the translated domain. In what follows, before we provide a brief overview of Bayesian inference using cINN, we explain the basics of normalizing flow.

3.4.1 Conditional invertible neural networks as a regression model for probabilistic estimation. Normalizing flows are generative techniques that can flexibly approximate any arbitrary probability distribution $f(\boldsymbol{\theta}|\boldsymbol{\beta})$ over a continuous domain. This is achieved by starting with a regular/base distribution $f_z(\mathbf{z})$ and applying a series of bijective transformations [36,37]. Let $\boldsymbol{\theta}$ be a vector of damage state variables and $\boldsymbol{\beta}$ be a vector denoting observations, as illustrated in Fig. 7, there are two types of flow transformation, namely generative direction and normalizing direction. In the *generative direction*, we can map a regular or base distribution $f_z(\mathbf{z})$ (e.g., Gaussian distribution) to an irregular distribution. This allows for the generation of samples of $\boldsymbol{\theta}$ from distribution $f(\boldsymbol{\theta}|\boldsymbol{\beta})$ by sampling $\mathbf{z}$ from distribution $f_z(\mathbf{z})$. In the *normalizing direction*, we can operate the opposite by transforming an irregular distribution to a normal form of the base distribution $f_z(\mathbf{z})$.

A key to enable the above bijective transformations is an invertible function $\boldsymbol{\theta} = M(\mathbf{z})$, where $M(\cdot)$ is an invertible function and both $M(\cdot)$ and $M^{-1}(\cdot)$ are differentiable. If such a invertible and differentiable function exists, we can compute the probability

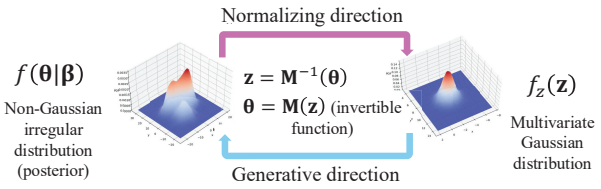

Fig. 7 Transformation of distributions in generative models [39]

density function $f(\boldsymbol{\theta}|\boldsymbol{\beta})$ of $\boldsymbol{\theta}$ as

$$\begin{aligned} f(\boldsymbol{\theta}|\boldsymbol{\beta}) &= f_z(\mathbf{z})|\det\ J_M(\mathbf{z})|^{-1} \\ &= f_z(M^{-1}(\boldsymbol{\theta}))\left|\det\ J_{M^{-1}}(\boldsymbol{\theta})\right|, \end{aligned} \tag{22}$$

where $\mathbf{z} = M^{-1}(\boldsymbol{\theta})$, $J_M(\mathbf{z})$ is the Jacobian matrix of $\boldsymbol{\theta} = M(\mathbf{z})$, and $J_{M^{-1}}(\boldsymbol{\theta})$ is the Jacobian of $M^{-1}(\cdot)$.

In practice, the invertible function $\boldsymbol{\theta} = M(\mathbf{z})$ is usually not directly available or explicitly defined. The added complexity of translating the domain of the observations further complicates the construction of such functions. One approach to overcome the challenge of constructing the invertible function is to learn the function based on data using invertible neural networks (INN) [40–42]. INNs are neural network architectures proposed in Ref. [43]. The basic building block of an INN is the affine coupling block as illustrated in Fig. 8. Each block consists of two complementary affine coupling layers that split the input vector $\boldsymbol{\omega}$ into two halves, namely $\boldsymbol{\omega}_1$ and $\boldsymbol{\omega}_2$. The split inputs are then transformed by an affine function using element-wise multiplication and addition to become inputs of the next block as follows [40]

$$\begin{aligned} \boldsymbol{\alpha}_1 &= \boldsymbol{\omega}_1 \odot \exp(s_2(\boldsymbol{\omega}_2)) + t_2(\boldsymbol{\omega}_2), \\ \boldsymbol{\alpha}_2 &= \boldsymbol{\omega}_2 \odot \exp(s_1(\boldsymbol{\alpha}_1)) + t_1(\boldsymbol{\alpha}_1), \end{aligned} \tag{23}$$

where $\odot$ is element-wise multiplication.

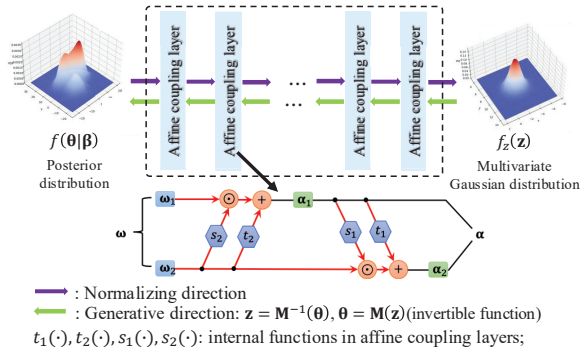

Fig. 8 Illustration of a cINN model as a regression model for Bayesian inference

Similar to Eq. (23), the inverse direction operation can also be easily performed using the affine coupling blocks. By stacking multiple blocks together, the invertible neural networks can approximate the invertible function $\boldsymbol{\theta} = M(\mathbf{z})$. By further integrating the INN model architecture with an additional neural network, we can approximate the posterior distribution $f(\boldsymbol{\theta}|\boldsymbol{\beta})$, which represents the conditional probability of $\boldsymbol{\theta}$ given the observations $\boldsymbol{\beta}$. This integrated architecture is known as a conditional invertible neural network (cINN) [44]. Consequently, the cINN model serves as a probabilistic regression model for Bayesian inference. For more detailed information on INN and cINN, we refer interested readers to Refs. [40] and [41].

3.4.2 Training a cINN model based on domain translation. Let $\hat{\boldsymbol{\lambda}}$ represent the parameters of the cINN model $\mathbf{z} = \gamma_{\boldsymbol{\lambda}}(\boldsymbol{\theta}; \boldsymbol{\beta})$, which include both the INN for bijective mapping and an additional neural network for conditioning. These parameters are estimated by solving the following optimization problem

$$\begin{aligned}\hat{\boldsymbol{\lambda}} &= \arg\min_{\boldsymbol{\lambda}} \mathbb{E}_{p(\boldsymbol{\beta})} \left[\mathbb{KL}(f(\boldsymbol{\theta}|\boldsymbol{\beta}) \,\|\, f_{\boldsymbol{\lambda}}(\boldsymbol{\theta}|\boldsymbol{\beta}))\right], \\ &= \arg\min_{\boldsymbol{\lambda}} \iint f(\boldsymbol{\theta}, \boldsymbol{\beta}) \log\{f_{\boldsymbol{\lambda}}(\boldsymbol{\theta}|\boldsymbol{\beta})\} \mathbf{d}\boldsymbol{\beta}\mathbf{d}\boldsymbol{\theta},\end{aligned} \tag{24}$$

where $\mathbb{E}(\cdot)$ represents expectation and $\mathbb{KL}(\cdot)$ is the Kullback–Leibler (KL) divergence between the true and the approximate posterior distributions.

The objective function of the above equation can be approximated by a Monte Carlo estimate as follows [41]

$$\hat{\boldsymbol{\lambda}} = \arg\min_{\boldsymbol{\lambda}} \frac{1}{N_o} \sum_{j=1}^{N_o} \left(\frac{\left\| \gamma_{\boldsymbol{\lambda}}(\boldsymbol{\theta}^{(j)}; \boldsymbol{\beta}^{(j)}) \right\|_2^2}{2} - \log \left| \det J_{\gamma_{\boldsymbol{\lambda}}}^{(j)} \right| \right), \tag{25}$$

where N_o is the number of training data and $J_{\gamma_{\boldsymbol{\lambda}}}^{(j)}$ is the Jacobian of $\mathbf{z} = \gamma_{\boldsymbol{\lambda}}(\boldsymbol{\theta}; \boldsymbol{\beta})$ evaluated at the j-th sample of $\boldsymbol{\theta}$ and $\boldsymbol{\beta}$.

If the CycleGAN-based approach (i.e., Sec. 3.3.1) is employed to translate the observations of the target miter gate to that of the source miter gates, we have the training data as $\{\boldsymbol{\theta}_{\text{sr},j}, j = 1, \cdots, N_{os}\}$ and $\{\boldsymbol{\beta}^{(j)} \doteq \hat{\mathbf{y}}_{o,\text{sr2sr},j}, j = 1, \cdots, N_{os}\}$. If DANN-based approach (i.e., Sec. 3.3.2) is employed to perform observation translation, we have the training data as $\{\boldsymbol{\theta}_{\text{sr},j}, j = 1, \cdots, N_{os}\}$ and $\{\boldsymbol{\beta}^{(j)} \doteq \boldsymbol{\eta}_{\text{DANN,sr},j}, j = 1, \cdots, N_{os}\}$ in Eq. (25). After the estimation of $\hat{\boldsymbol{\lambda}}$, the trained cINN model can be used to approximate the posterior distribution of $\hat{f}(\boldsymbol{\theta}|\boldsymbol{\beta})$ for given observation $\boldsymbol{\beta}$.

3.4.3 Damage diagnostics using Bayesian inference in the translated domain. Once a cINN model has been successfully trained in the translated domain, we can generate samples from the posterior distribution of the damage state for any given observation $\boldsymbol{\beta}$ of the target miter gate. This is achieved by first generating N_{MCS} samples of $\mathbf{z}$ from $f_z(\mathbf{z})$. Let the samples be $\{\mathbf{z}^{(i)}, i = 1, \cdots, N_{MCS}\}$, then we have the posterior samples of $\hat{f}(\boldsymbol{\theta}|\boldsymbol{\beta})$ using the cINN model as

$$\boldsymbol{\theta}^{(i)} = \gamma_{\boldsymbol{\lambda}}^{-1}(\mathbf{z}^{(i)}; \boldsymbol{\beta}), i = 1, \cdots, N_{MCS}, \tag{26}$$

where $\gamma_{\boldsymbol{\lambda}}^{-1}(\cdot)$ stands for the generative direction of operation of the model, $\boldsymbol{\beta}$ is $\hat{\mathbf{y}}_{o,\text{tg2sr},j}, j = 1, \cdots, N_{ot}$, if CycleGAN-based approach is employed for domain translation and is $\boldsymbol{\eta}_{\text{DANN,tg},i}$ if DANN-based approach is used.

Based on the posterior samples, the posterior distribution $f_{DT}(\boldsymbol{\theta}_{\text{tg},i})$ (i.e., given in Eq. (9)) of the damage state can be obtained using domain translation by leveraging information from similar, but different miter gates.

3.5 Bayesian model averaging for the integration of different estimations. As discussed in Sec. 3.2 and depicted in Fig. 4, we can also conduct damage diagnostics using Bayesian inference through computational simulation of the target miter gate. This method complements the previously described diagnostics based on domain translation. In this section, we first introduce damage diagnostics utilizing physics-based Bayesian inference. Subsequently, we explore the integration of estimations from different approaches through Bayesian model averaging.

3.5.1 Damage diagnostics using physics-based Bayesian inference. In damage diagnostics using physics-based computational simulation, we calibrate the damage variable of the simulation model to minimize the discrepancy between the model prediction and actual observations. A commonly used approach to solve such an inverse problem using computational simulation is Bayesian inference or Bayesian model updating [45], which estimates the damage state as follows

$$\begin{aligned}&f_{\boldsymbol{\theta}|\mathbf{y}}(\boldsymbol{\theta}_{\text{tg},i}|\mathbf{y}_{o,\text{tg},i}, \mathbf{u}_{\text{tg},i}; \mathbb{G}) \\ &\propto L_{\mathbf{y}|\boldsymbol{\theta}}(\mathbf{y}_{o,\text{tg},i}|\boldsymbol{\theta}_{\text{tg},i}, \mathbf{u}_{\text{tg},i}; \mathbb{G}) f_{\boldsymbol{\theta}}(\boldsymbol{\theta}_{\text{tg},i}),\end{aligned} \tag{27}$$

where $f_{\boldsymbol{\theta}}(\boldsymbol{\theta}_{\text{tg},i})$ is the prior distribution of the damage state and $L_{\mathbf{y}|\boldsymbol{\theta}}(\mathbf{y}_{o,\text{tg},i}|\boldsymbol{\theta}_{\text{tg},i}, \mathbf{u}_{\text{tg},i}; \mathbb{G})$ is a likelihood function computed using the computational model $\mathbb{G}$ (i.e., $\mathbf{y}_{\text{tg}} = G(\boldsymbol{\theta}, \mathbf{u})$) by considering uncertainty sources. Fig. 9 shows an example of a computational simulation model of structural analysis for a miter gate.

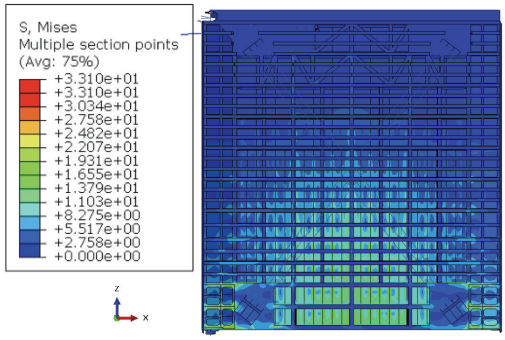

Fig. 9 An example of FEA model of miter gates

If the major uncertainty sources considered are the observation noises which could include both the sensor measurement noises and

the uncertainty in the model prediction due to unmodeled physics, the likelihood function given in Eq. (27) can be derived as [46]

$$L_{\mathbf{y}|\boldsymbol{\theta}}(\mathbf{y}_{o,\mathrm{tg},i}|\boldsymbol{\theta}_{\mathrm{tg},i}, \mathbf{u}_{\mathrm{tg},i}; \mathbb{G}) = \frac{\exp\left(-0.5(\mathbf{y}_{o,\mathrm{tg},i} - \mathbf{y}_{\mathrm{tg},i})^T \boldsymbol{\Sigma}^{-1}(\mathbf{y}_{o,\mathrm{tg},i} - \mathbf{y}_{\mathrm{tg},i})\right)}{\sqrt{(2\pi)^{N_t \times N_s}\,|\boldsymbol{\Sigma}|}}, \tag{28}$$

in which $\boldsymbol{\Sigma}$ is the covariance matrix which is usually modeled as a diagonal matrix with the diagonal elements being the unknown variance σ_ε^2 of the observation noises, and $\mathbf{y}_{\mathrm{tg},i} \in \mathbb{R}^{N_t \times N_s}$ is the predicted strain response using the physics-based simulation model $\mathbb{G}$. In this paper, the unknown variance σ_ε^2 is also treated as part of the estimation parameters $\boldsymbol{\theta}$ which includes both the gap length and the observation noise variance.

Once the likelihood function is derived, the posterior distribution of the target miter gate's damage state, as given in Eq. (27), can be estimated using various Bayesian methods, such as Markov Chain Monte Carlo simulation and particle filtering [12,47]. While the physics-based Bayesian inference method can estimate the posterior distribution of the damage state, this estimate may be biased due to imperfections in the physics-based simulation model, such as the unmodeled physics due to misunderstanding or simplification, numerical discretization error, etc. Although numerous approaches have been developed over the past decades to address model uncertainty in Bayesian model calibration [29,48–50], the bias in posterior distribution estimation can only be mitigated, not eliminated. Furthermore, a limited number of observations or monitoring data for the target miter gate can introduce additional bias or significantly increase uncertainty in the damage state estimation.

The method proposed in Sec. 3.4 offers a data-driven alternative to estimating the posterior distribution of the damage state for the target miter gate, based on domain translation and normalizing flows. By leveraging inspection and monitoring data from similar, but different, miter gates, this approach bypasses the need for a physics-based simulation model of the target miter gate. Consequently, it has the potential to overcome the limitations and disadvantages associated with physics-based methods (i.e., Sec. 3.5.1), as well as the constraint posed by the limited monitoring data for the target gate. Given that both approaches have their own strengths and weaknesses, we will next discuss how to combine their estimations to achieve a final posterior distribution estimation of the damage state for the target miter gate.

3.5.2 Bayesian model averaging for damage diagnostics. In this paper, we combine the posterior distribution from the two different approaches above through a Bayesian model averaging framework. Note that there are actually three approaches/models if we consider the two different domain translation methods as two different variants. The three approaches are (1) the CycleGAN-based method, (2) the DANN-based method, and (3) the physics-based Bayesian inference method. The Bayesian model averaging of the results from different methods avoids the risk of double-counting the monitoring data of the target miter gate in Bayesian damage diagnostics. In the Bayesian model averaging setting, we have the final estimation of the posterior distribution of the damage state as

$$\begin{aligned} &f(\boldsymbol{\theta}_{\mathrm{tg},i}|(\tilde{\mathbf{y}}_{o,\mathrm{sr}}, \tilde{\boldsymbol{\theta}}_{\mathrm{sr}}, \mathbf{y}_{o,\mathrm{tg},i}; \mathbb{G})) \\ &\approx f_{DT}(\boldsymbol{\theta}_{\mathrm{tg},i}; \mathbb{H}_{\mathrm{CG}}) p(\mathbb{H}_{\mathrm{CG}}|\mathbf{D}) \\ &+ f_{DT}(\boldsymbol{\theta}_{\mathrm{tg},i}; \mathbb{H}_{\mathrm{DN}}) p(\mathbb{H}_{\mathrm{DN}}|\mathbf{D}) \\ &+ f(\boldsymbol{\theta}_{\mathrm{tg},i}|(\mathbf{y}_{o,\mathrm{tg},i}, \mathbf{u}_{\mathrm{tg},i}; \mathbb{G})) p(\mathbb{G}|\mathbf{D}), \end{aligned} \tag{29}$$

where $f_{DT}(\boldsymbol{\theta}_{\mathrm{tg},i}; \mathbb{H}_{\mathrm{CG}})$ represents the posterior distribution of the damage state estimated based on domain translation using CycleGAN and normalizing flow using historical data from source miter gates (i.e., Secs. 3.3 and 3.4), $f_{DT}(\boldsymbol{\theta}_{\mathrm{tg},i}; \mathbb{H}_{\mathrm{DN}})$ denotes the posterior distribution obtained using DANN-based domain translation, $f(\boldsymbol{\theta}_{\mathrm{tg},i}|(\mathbf{y}_{o,\mathrm{tg},i}, \mathbf{u}_{\mathrm{tg},i}; \mathbb{G}))$ is the posterior distribution obtained using physics-based method in Sec. 3.5.1, and $p(\mathbb{H}_{\mathrm{CG}}|\mathbf{D})$, $p(\mathbb{H}_{\mathrm{DN}}|\mathbf{D})$, and $p(\mathbb{G}|\mathbf{D})$ are weights of the three different approaches, which are respectively given by

$$p(\mathbb{G}|\mathbf{D}) = \frac{p(\mathbf{D}|\mathbb{G})P(\mathbb{G})}{p(\mathbf{D})}, \tag{30}$$

$$p(\mathbb{H}_{\mathrm{CG}}|\mathbf{D}) = \frac{p(\mathbf{D}|\mathbb{H}_{\mathrm{CG}})P(\mathbb{H}_{\mathrm{CG}})}{p(\mathbf{D})}, \tag{31}$$

and

$$p(\mathbb{H}_{\mathrm{DN}}|\mathbf{D}) = \frac{p(\mathbf{D}|\mathbb{H}_{\mathrm{DN}})P(\mathbb{H}_{\mathrm{DN}})}{p(\mathbf{D})}, \tag{32}$$

where $P(\mathbb{G})$, $P(\mathbb{H}_{\mathrm{CG}})$, and $P(\mathbb{H}_{\mathrm{DN}})$ are the prior weights of the three methods. Without any additional information available, we can assign equal weights to all approaches, and $p(\mathbf{D})$ is given by

$$\begin{aligned} p(\mathbf{D}) &= p(\mathbf{D}|\mathbb{G})P(\mathbb{G}) + p(\mathbf{D}|\mathbb{H}_{\mathrm{CG}})P(\mathbb{H}_{\mathrm{CG}}) \\ &+ p(\mathbf{D}|\mathbb{H}_{\mathrm{DN}})P(\mathbb{H}_{\mathrm{DN}}). \end{aligned} \tag{33}$$

In the above equations, $p(\mathbf{D}|\mathbb{G})$ can be easily computed based on Eq. (28) as

$$p(\mathbf{D}|\mathbb{G}) = \int L_{\mathbf{y}|\boldsymbol{\theta}}(\mathbf{y}_{o,\mathrm{tg},i}|\boldsymbol{\theta}_{\mathrm{tg},i}, \mathbf{u}_{\mathrm{tg},i}, \mathbb{G}) f_{\boldsymbol{\theta}}(\boldsymbol{\theta}_{\mathrm{tg},i}|\mathbb{G}) d\boldsymbol{\theta}_{\mathrm{tg},i}, \tag{34}$$

where $f_{\boldsymbol{\theta}}(\boldsymbol{\theta}_{\mathrm{tg},i}|\mathbb{G})$ is the prior distribution of $\boldsymbol{\theta}_{\mathrm{tg},i}$ when the computational simulation model $\mathbb{G}$ is employed for Bayesian model updating. In this paper, a non-informative uniform prior distribution is used.

The estimation of $p(\mathbf{D}|\mathbb{H}_{\mathrm{CG}})$ and $p(\mathbf{D}|\mathbb{H}_{\mathrm{DN}})$ can be accomplished similarly. Taking $p(\mathbf{D}|\mathbb{H}_{\mathrm{CG}})$ as an example, we can compute $p(\mathbf{D}|\mathbb{H}_{\mathrm{CG}})$ as follows

$$p(\mathbf{D}|\mathbb{H}_{\mathrm{CG}}) = \int f_H(\boldsymbol{\eta}_{o,\mathrm{tg},i}|\boldsymbol{\theta}_{\mathrm{tg},i}, \mathbb{H}_{\mathrm{CG}}) f_{\boldsymbol{\theta}}(\boldsymbol{\theta}_{\mathrm{tg},i}|\mathbb{H}_{\mathrm{CG}}) d\boldsymbol{\theta}_{\mathrm{tg},i}, \tag{35}$$

in which $f_H(\boldsymbol{\eta}_{o,\mathrm{tg},i}|\boldsymbol{\theta}_{\mathrm{tg},i}, \mathbb{H}_{\mathrm{CG}})$ is the likelihood of observing $\boldsymbol{\eta}_{o,\mathrm{tg},i}$ (i.e., $\hat{\mathbf{y}}_{o,\mathrm{tg2sr},i}$ if CycleGAN is employed for domain translation) in the translated domain for given $\boldsymbol{\theta}_{\mathrm{tg},i}$, and $f_{\boldsymbol{\theta}}(\boldsymbol{\theta}_{\mathrm{tg},i}|\mathbb{H}_{\mathrm{CG}})$ is the prior distribution of $\boldsymbol{\theta}_{\mathrm{tg},i}$ when the domain translation model $\mathbb{H}_{\mathrm{CG}}$ is employed for Bayesian damage diagnostics.

However, $f_H(\boldsymbol{\eta}_{o,\mathrm{tg},i}|\boldsymbol{\theta}_{\mathrm{tg},i}, \mathbb{H}_{\mathrm{CG}})$ in Eq. (35) is not explicitly known due to the complicated domain translation and the analytically intractable relationship between $\boldsymbol{\theta}_{\mathrm{tg},i}$ and $\boldsymbol{\eta}_{o,\mathrm{tg},i}$. It poses a significant challenge to the Bayesian model averaging given in Eq. (29). To tackle this challenge, this paper employs a normalizing flow-based approach to estimate the intractable likelihood [51,52]. It is based on the change of variables in generative modeling. Similar to the estimation of the posterior distribution in Sec. 3.4.1 (i.e., Eq.(22)), a normalizing flow model is constructed to estimate the likelihood function as follows

$$\begin{aligned} f(\boldsymbol{\eta}|\boldsymbol{\theta}) &= f_z(\mathbf{z}_\eta)\left|\det\, J_{M_\eta}(\mathbf{z})\right|^{-1} \\ &= f_z({M_\eta}^{-1}(\boldsymbol{\eta}))\left|\det\, J_{{M_\eta}^{-1}}(\boldsymbol{\eta})\right|, \end{aligned} \tag{36}$$

where $M_\eta(\cdot)$ represents the invertible function constructed using cINN for the estimation of $f(\boldsymbol{\eta}|\boldsymbol{\theta})$. In this paper, the Bayesflow Python library is employed to learn the likelihood function estimator [52].

Once we have estimated the likelihood function $f(\boldsymbol{\eta}|\boldsymbol{\theta})$ using Eqs. (28) and (36), we can determine the final estimation of the damage state through Bayesian model averaging as given in Eq. (29). Additionally, we can also perform model selection using Bayes factor (i.e., Bayesian Hypothesis Testing) based on Eqs. (34) and (35) as

$$B_{GC} = \frac{p(\mathbf{D}|\mathbb{G})}{p(\mathbf{D}|\mathbb{H}_{\text{CG}})}, \; B_{GD} = \frac{p(\mathbf{D}|\mathbb{G})}{p(\mathbf{D}|\mathbb{H}_{\text{DN}})}, \\ B_{\text{CD}} = \frac{p(\mathbf{D}|\mathbb{H}_{\text{CG}})}{p(\mathbf{D}|\mathbb{H}_{\text{DN}})}, \tag{37}$$

where B_{GC}, B_{GD}, and B_{CD} are respectively Bayes factor for pairwise model comparison between physics-based method and domain translation using CycleGAN, and physics-based method and domain translation using DANN, and CycleGAN-based method and DANN-based method.

Up to this point, we have discussed all the details of the proposed framework, which is summarized in Fig. 4. In Sec. 4, we will demonstrate the application of this framework with a case study.

4 Case Study

4.1 Problem description. In this section, the proposed damage diagnostics framework is applied to two similar but different miter gates to demonstrate its efficacy. As depicted in Fig. 10, the two miter gates located upstream and downstream of the same basin have been chosen to serve as the source and target miter gates, respectively.

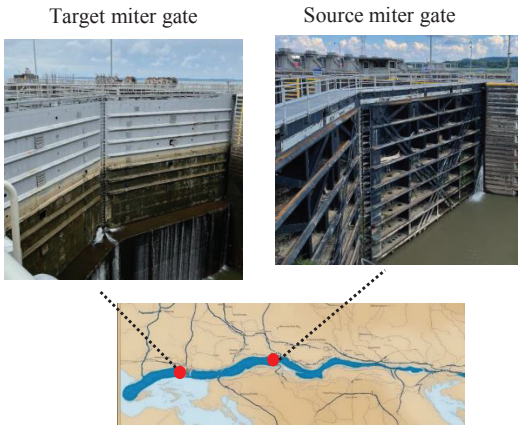

Fig. 10 Illustration of source and target miter gates on a river.

To verify the efficacy of the proposed BiEDT framework and due to the lack of real-world data, synthetic observations are generated for the miter gates. In this paper, the observations of both the source and target miter gates are generated through a physics-based finite element analysis (FEA) model by adding noises. Noise is introduced to the observation data to reflect the variability and imperfections typically found in actual measurements.

Let $\mathbf{s}_i$ represent the i-th simulated strain measurements of the source miter gates from the model given in Fig. 9. The strain observations of the source miter gates, denoted as $\mathbf{y}_{o,\text{sr},i}$, can be described by the following equation $\mathbf{y}_{o,\text{sr},i} = \mathbf{s}_i + \boldsymbol{\epsilon}_i$, where $\boldsymbol{\epsilon}_i$ is the noise term added to each strain measurement and $\boldsymbol{\epsilon}_i$ follows a normal distribution with a mean of 0 and a standard deviation that is a function of the magnitude of the corresponding strain measurement. Specifically: $\boldsymbol{\epsilon}_i \sim \mathcal{N}(0, 0.01 \times |\mathbf{s}_i|)$. The strain response of the target miter gate is hypothetically derived by altering the response from the source miter gates. This modification ensures that while the two miter gates are relevant or share similarities, they remain different. The simulation model of the target miter gate is defined as follows

$$\mathbf{y}_{\text{tg},i} = \mathbf{s}_i(\cos(350\mathbf{s}_i) + \sin(650\mathbf{s}_i)). \tag{38}$$

The observation model of the target miter gate is given by

$$\mathbf{y}_{o,\text{tg},i} = \mathbf{s}_i(\cos(500\mathbf{s}_i) + \sin(800\mathbf{s}_i)) + \boldsymbol{\epsilon}_{\text{tg},i}, \tag{39}$$

where $\boldsymbol{\epsilon}_{\text{tg},i} \sim \mathcal{N}(0, 0.01 \times |\mathbf{s}_i|)$ is the observation noise of the target miter gate. As we can see from the above two equations that the simulation model is different from the observation model to mimic model form uncertainty that is inherent in computational simulation models.

The strain responses of the two miter gates (specifically, the source and target miter gates) are affected by their damage states (such as gap length) and water levels. The water levels at the two miter gates are different and are modeled using an Autoregressive Moving Average (ARMA) model. It is assumed that each miter gate has eight strain gauges (i.e., $N_s = 8$). Using the above-defined observation models, we generate 200 datasets of strain observations for the source miter gates (i.e., $N_{os} = 200$), and 180 datasets of strain observations for the target miter gate with unknown damage states (i.e., $N_{ot} = 180$). Each dataset consists of strain observation data of eight strain gauges over twenty time steps (i.e., $N_t = 20$). The damage states (i.e., gap length) corresponding to the 200 datasets of the source miter gates are different and are available from historical inspections. Their counterparts of the target miter gate are unknown and are to be estimated.

As mentioned earlier, the observations of different miter gates are inherently related but different. This similarity and difference can be observed when comparing both the water level data and the strain observations. Fig. 11 shows the differences in upstream and downstream water levels between the source and target miter gates. It is important to note that the difference in water levels, particularly the downstream water levels, are not very significant. This is because we assume that the operational conditions of the two miter gates are similar and related, since they operate on the same river. Following that, Fig. 12 presents a comparison of the monitoring data from the source and target miter gates. The data clearly shows that even though the operational conditions are very similar, the strain responses are quite different due to structural differences between the two miter gates. Fig. 13 presents a comparison of the strain data from sensors placed on both the source and target miter gates, illustrating very different distributions for the same sensors across different structures. The top graph illustrates the strain readings between Sensor 1 and Sensor 2, while the bottom graph compares the data from Sensor 1 and Sensor 3. From the figure, it can be seen that the strain responses for corresponding sensors vary significantly between the two gates. The data points from the source miter gate, represented in red, form a cluster different from those of the target miter gate, shown in blue.

In addition to the differences highlighted in Figs. 11, 12, and 13, we calculate the Structural Similarity Index (SSIM) and Root Mean Square Error (RMSE) between the monitoring data of the source miter gate and the target miter gate. The average SSIM between the data of the source and targe miter gates is 0.4429, and the RMSE is 0.4231. These values are noticeably lower than those for the comparison between synthetic and real miter gate measurement data, as shown in Table 2. This quantification highlights the differences and similarities between the two types of miter gates in the case study. It is important to note that we have not yet established a standard threshold for similarity between miter gates, which is essential for applying the methods discussed in this paper for practical applications. Developing an effective similarity metric and determining an appropriate threshold to ensure the effectiveness of the proposed framework will be the focus of our future research.

The objective of this study is to accurately estimate the damage state of the target miter gate by leveraging strain observations and the inspected damage states of the source miter gates. It is worth

mentioning that while the true damage state is used to generate these observations of the target miter gate, it is assumed to be unknown during the actual process of damage diagnostics.

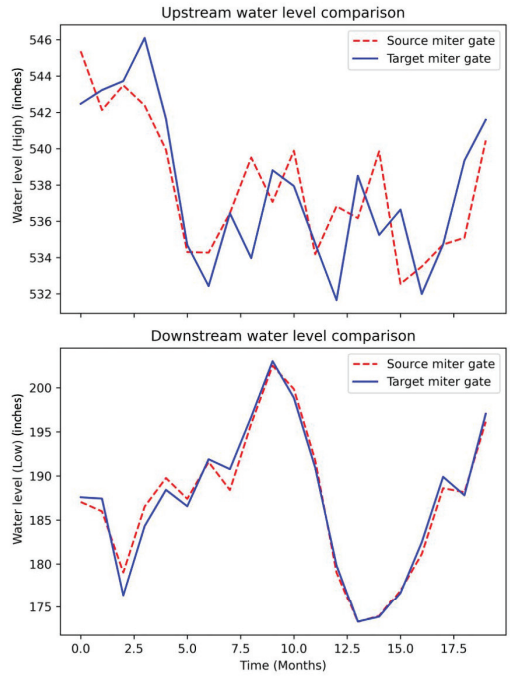

Fig. 11 Water level comparison of source and target miter gates

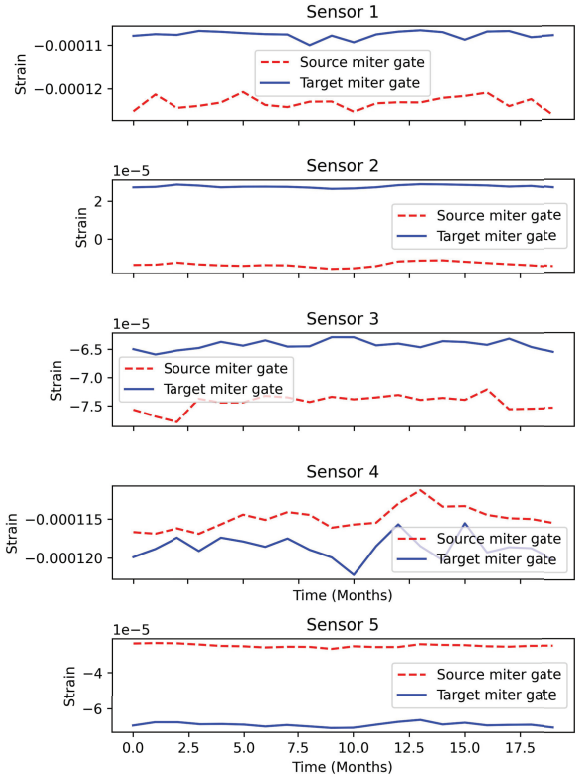

Fig. 12 A comparison of monitoring data of source and target miter gates (Data of only five sensors are plotted for illustration purpose)

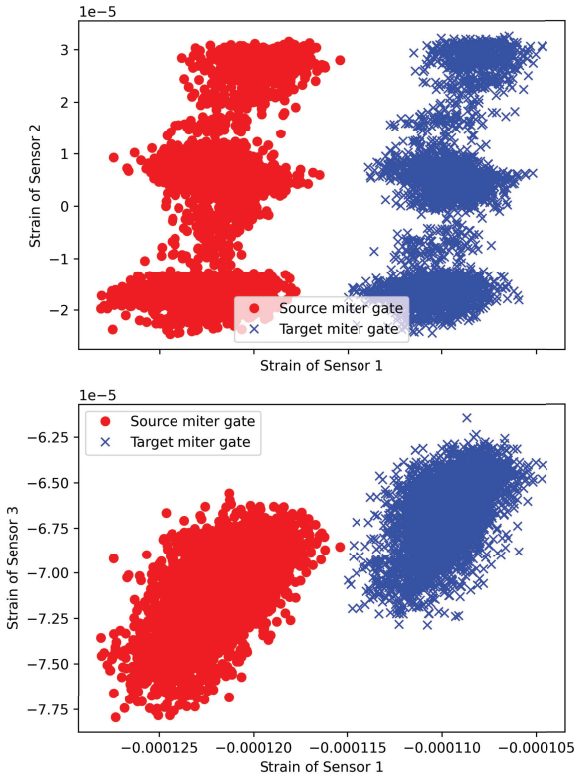

Fig. 13 Scatter plot comparison of monitoring data of the source and target miter gates

4.2 Domain translation of the observations.

4.2.1 CycleGAN-based domain translation. CycleGAN is first employed to perform domain adaptation/translation on the data from the target miter gate using the data from the source miter gates. During the training phase, the model establishes a relationship between data from two different miter gates by utilizing data from the source miter gate as input and data from the target miter gate as output. The training process for the CycleGAN model involves several key steps. Preprocessing is first performed to transform the raw data into a format suitable for image-based analysis. This preprocessing phase includes sorting the data, normalizing it, and ultimately converting it to image format. Specifically, in this study, the data is sorted based on the highest strain response values across the samples. This approach is adopted because the gap length significantly influences the strain response values, ensuring that the CycleGAN can accurately learn the relationships between the two different domains. After the data is sorted, it undergoes normalization to limit the range of data values, and then it is converted into an image format. Each data sample is represented as an image, with the two dimensions corresponding to time steps and sensor indices. Following preprocessing, this image-formatted data is used as the input for training the CycleGAN.

Table 1 presents the hyper-parameters for the training of CycleGAN. In the evaluation of CycleGAN's performance for domain translation, specifically in transforming images related to miter gate observations, we adopt three key metrics: SSIM, RMSE, and Fréchet Inception Distance (FID). These metrics are crucial for validating the effectiveness of CycleGAN in performing realistic and accurate image translations. Additionally, we focus on evaluating the capability of CycleGAN under three different scenarios: (1) Synthetic Source vs. Real Source: This comparison assesses the ability of CycleGAN to generate synthetic image data of source miter gates from the target miter gate. (2) Original Source vs.

Reconstructed Source. (3) Target vs. Reconstructed Target. Table 2 shows those comparison results for CycleGAN performance evaluation. Overall, these scores affirm that CycleGAN trains well and is effective in generating realistic and structurally consistent translated data.

Table 1 Model parameters of CycleGAN

Variable Name	Conv U-net
Number of epochs	3000
Batch size	5
Learning rate for generators	0.0001
Learning rate for discriminators	0.0001
Dropout	0.1
$\mathcal{L}_{\text{cyc}}$ (cycle consistency loss)	20
$\mathcal{L}_{\text{id}}$ (identity loss)	10
Optimizer	Adam

Table 2 Comparison of metrics for different objects after using CycleGAN

Object of Comparison	SSIM	RMSE	FID
Syn_source vs. Real_source	0.8000	0.0808	0.9247
Real_source vs. Reconst_source	0.9649	0.0572	0.4020
Real_target vs. Reconst_target	0.9294	0.0709	0.7108

Fig. 14 presents the results of domain adaptation using CycleGAN. The figure contains two graphs; the upper graph plots the strain readings from Sensor 1 against Sensor 2, and the lower graph compares the strain readings from Sensor 1 against Sensor 3. In these figures, the data from the source miter gate is marked with red circles, while the data translated from the target miter gate is represented by blue crosses. Notably, the figure shows that the synthetic source data, generated from the target miter gate using CycleGAN, appears to cluster closely with the actual observations of the source miter gates. This suggests that the CycleGAN has effectively adapted the domain of the target gate data to align with the data characteristics of the source miter gates. The overlapping clusters indicate a successful translation, where the adapted synthetic observations mimic the real observations of the source miter gates. This highlights the potential of CycleGAN in bridging the gap between different domains by generating synthetic yet realistic data representations.

4.2.2 DANN-based domain adaptation. The second domain adaptation model we explore is DANN. DANN performs domain adaptation by extracting domain-independent features from observations between source miter gates and the target miter gate. The label predictor and feature extractor are trained together iteratively, as different features extracted require a different label predictor. Note that only labels from the source miter gates are used in training label predictor while both observations from the source and target miter gates are used to train the feature extractor with a multi-layer discriminator. The discriminator forces the feature extractor to extract domain-independent features from both domains such that the discriminator can not distinguish them from the features. The observation data and labels (i.e., gap length of the source miter gates) are normalized with min-max normalization, respectively.

Table 3 shows the hyper-parameters for the training of the DANN model.

Fig. 15 shows the results of features extracted from the source and target miter gates. Among the 80 features, we depict the comparisons of feature pairs 2 vs. 4, 3 vs. 5, 2 vs. 6, and 3 vs. 7 for illustration purposes. Notably, for feature pairs 3 vs. 5 and 3 vs. 7, the features from the source domain are very close to those from the target domain, which shows the efficacy of the DANN approach. Consequently, the relation between these feature pairs remains consistent across both domains. Conversely,

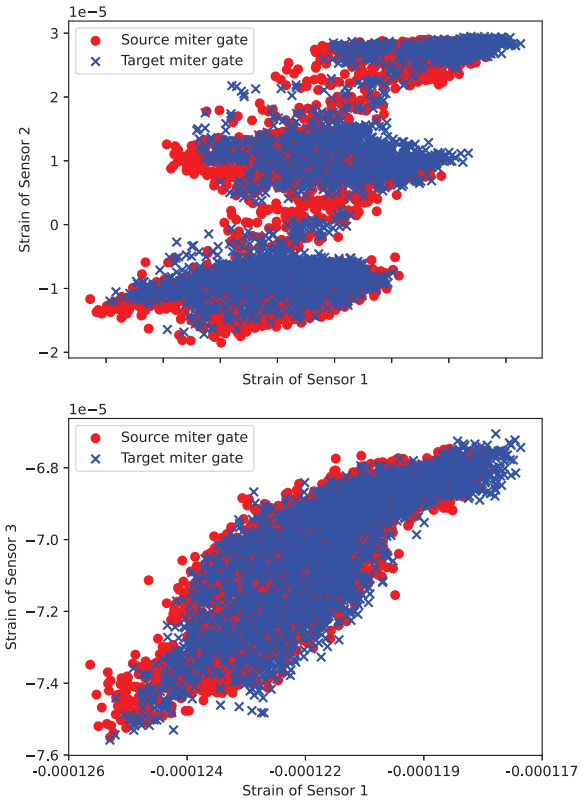

Fig. 14 Scatter plot comparison of monitoring data of source and target miter gates after observation translation using CycleGAN

Table 3 Model parameters of DANN

Variable Name	DANN
Number of epochs	1500
Batch size	16
Feature size	80
Learning rate for generators	0.001
Learning rate for discriminators	0.001
Optimizer	SGD

other feature pairs demonstrate significant differences between the source and target domains, resulting in a change in their relation from source to target. However, for feature pairs 2 vs. 4 and 2 vs. 6, while the points are generally close between both domains, there are noticeable differences. For example, feature 2 from the source miter gate shows a bidirectional relationship with changes in features 4 and 6. In contrast, feature 2 from the target miter gate appears to follow only one direction of change with these features.

4.3 Bayesian damage diagnostics in translated domain. Following the domain translations, cINN is employed to perform Bayesian inference in the two translated domains, respectively. Herein, cINN consists of three conditional affine coupling layers. Each conditional affine coupling layer contains four separate fully connected layer neural networks with exponential linear units. The entire training process goes through 500 epochs, each containing 100 iterations.

For illustrative purposes, Fig. 16 lists the comparison between the true value, the prior distribution, and the posterior distribution estimated by cINN and cycleGAN-based domain translation for the four gap lengths. It can be found that except for a slight deviation in gap 2, the estimated posterior distribution of the remaining three gaps well captures the information of the true value. Meanwhile,

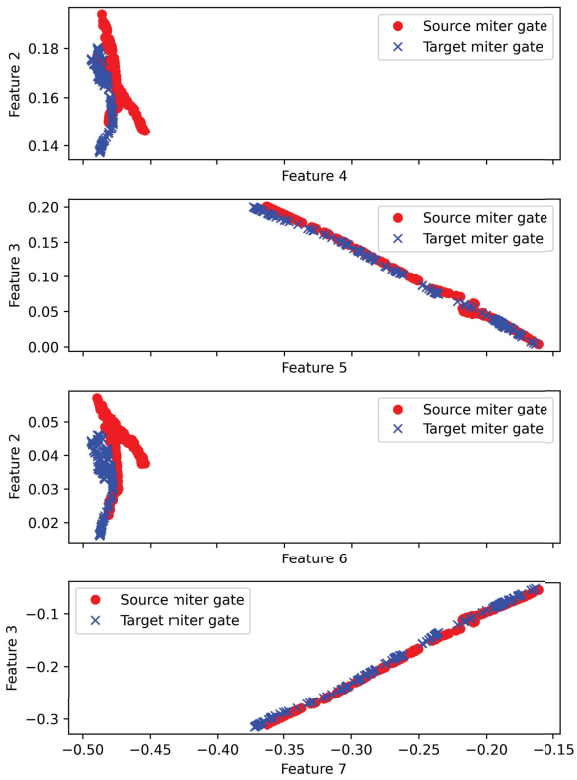

Fig. 15 Comparison of DANN features of the source and target miter gates

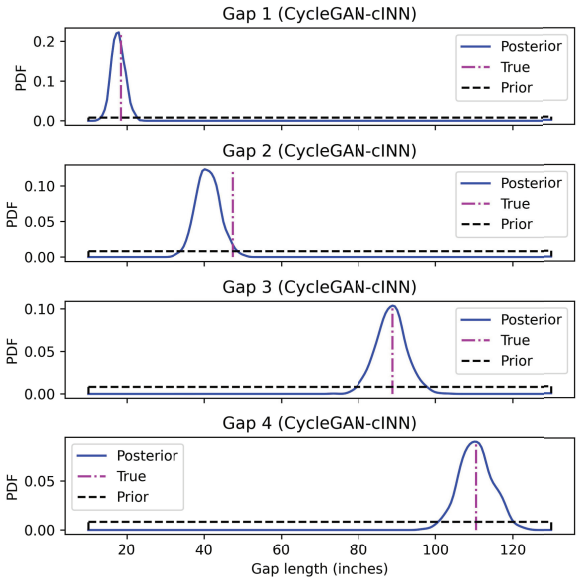

Fig. 16 Posterior distribution of gap length obtained using cINN and CycleGAN-based domain translation

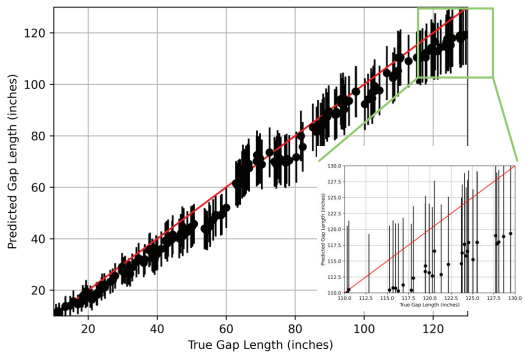

Fig. 17 Errorbar plot of the posterior distribution of different gap length estimates (CycleGAN-based domain translation)

Fig. 17 gives the errorbar plot of the posterior distribution estimated by cINN and cycleGAN-based domain translation for all gap lengths of the 180 obseravation datasets. Overall, the posterior mean is consistent with the true value, and the posterior variance does not show much fluctuation.

Following that, Fig. 18 presents the comparison between the true value, the prior distribution, and the posterior distribution estimated by cINN and DANN-based domain translation for the four gap lengths. Similar to the cycleGAN-based translation, except for gap 2, the posterior distributions match the true value very well for the other three gap lengths. Fig. 19 shows the errorbar plot of the posterior distribution estimated by cINN and DANN-based domain translation for all gap lengths. Different from the results of the cycleGAN-based method, the posterior estimations from cINN and DANN-based domain translation exhibit large fluctuations between 40 and 60, deviating from the true value.

4.4 Bayesian model averaging for damage diagnostics of miter gates.

4.4.1 Physics-based damage diagnostics using Bayesian method. As described in Sec. 3.5.1, we can also perform physics-based Bayesian inference for damage diagnostics, in addition to the above methods using domain translation and cINN. In the physics-based damage diagnostics using Bayesian inference, the prior distributions of the gap length and the standard deviation of the observation noises are non-informative uniform distributions, which are respectively $[10, 130]$ inches and $[3 \times 10^{-4}, 3 \times 10^{-4}]$. Fig. 20 presents the posterior distribution of gap lengths obtained from physics-based Bayesian inference for four illustrative datasets. From the results, we can see that the posterior distributions for gap lengths over 60 (as seen in Gap 3,4) show a high degree of accuracy, with the peak of the posterior probability density function closely aligning with the true value. The sharp, narrow peaks of the posterior distribution indicate high confidence in the estimates for large gap lengths. However, for smaller gaps (especially for Gap 1 and Gap 2), the posterior distributions do not align as closely with the true values. This misalignment indicates potential model error or limitations in the model's ability to estimate small gap lengths. The significant error in estimating smaller gap lengths could be attributed to the uncertain variance σ_ε^2 of the observation noises.

Fig. 21 presents an error-bar plot of the posterior distribution for various gap length estimates using physics-based Bayesian inference, showing a comparison between the predicted and true gap lengths. It shows that the model has a good predictive performance for larger gap lengths, as indicated by the clustering of points along the red line in the higher range. Fig. 21 corroborates the findings from the previous analysis (i.e., Fig. 20), where the model shows better accuracy for larger gap lengths and faces difficulties with smaller gaps.

4.4.2 Bayesian model averaging of posterior distributions. After implementing Bayesian damage diagnostics in the translated domain and using a physics-based model, we integrate these posterior distributions using a Bayesian model averaging framework.

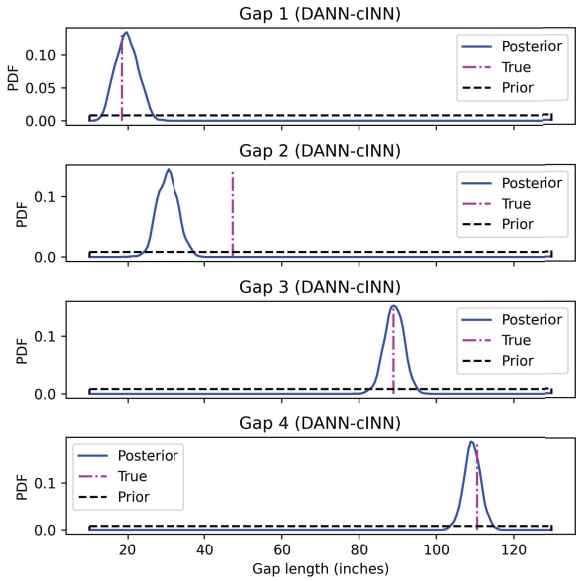

Fig. 18 Posterior distribution of gap length obtained using cINN and DANN-based domain translation

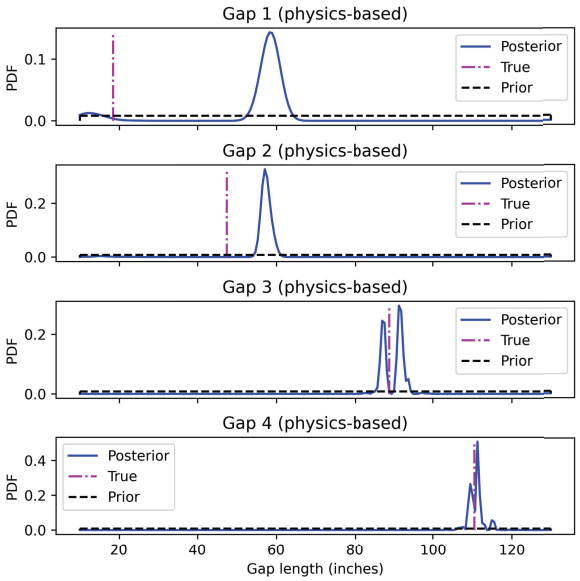

Fig. 20 Posterior distribution of gap length obtained using physics-based Bayesian inference

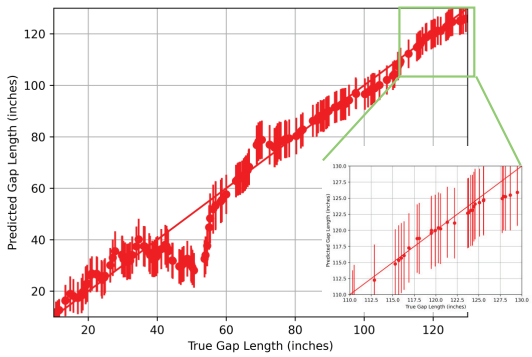

Fig. 19 Errorbar plot of the posterior distribution of different gap length estimates (DANN-based domain translation)

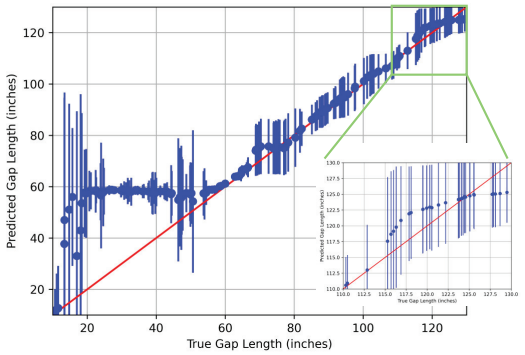

Fig. 21 Errorbar plot of the posterior distribution of different gap length estimates (Physics-based Bayesian inference)

This application of BMA using posterior distributions is obtained from three different approaches: CycleGAN-cINN, DANN-cINN, and physics-based approaches. Fig. 22 shows the combined posterior distributions for a gap length around 70. The posterior curves for each method (DANN-cINN, CycleGAN-cINN, Physics-based) indicate their individual estimations before averaging. The posterior distribution of the physics-based method exhibits a multimodal pattern. This phenomenon may be attributed to the large uncertainty in the variance of the observation noises. As mentioned above, the prior distribution of σ_ε is $[3\times10^{-4}, 3\times10^{-4}]$. It leads to a certain identifability issue for the physics-based method. The BMA curve, which is the combined result of these three approaches, seeks to average the estimates of each method. The bar chart on the right illustrates the weights assigned to each method in the BMA process (i.e., Eqs. (30)-(32)). It shows that in this case, the physics-based method has the highest weight, suggesting its predictions are considered the most reliable for this particular gap length scenario based on the likelihood estimates.

Fig. 23 represents a different gap length scenario around 125. Similar to Fig. 22, it compares the posterior estimates from the three methods alongside their BMA result. The weights are notably different; the DANN-cINN method is given the most weight, indicating its superior performance or reliability for this larger gap scenario.

Fig. 24 shows the predicted versus true gap lengths for each method after using the proposed model selection method (see Sec. 3.5.2). It shows the predictive accuracy of each method across the entire range of gap lengths. By integrating the results of different methods through model selection using the Bayes factor, we aim to mitigate the individual limitations of each method, leveraging their combined strengths to enhance predictive accuracy. As indicated in this figure, the CycleGAN-based method is selected when the gap length is small and the DANN-based is selected when the gap length is large. For the other regions, the physics-based Bayesian inference method is selected. Results in this figure demonstrate the efficacy of the proposed approach in combining different Bayesian diagnostic models to provide a robust estimation of gap lengths, which is crucial for accurate damage assessment in structural health monitoring.

5 Conclusions and Discussion

This paper presents a novel BiEDT framework, for damage diagnostics that integrates domain translation with Bayesian in-

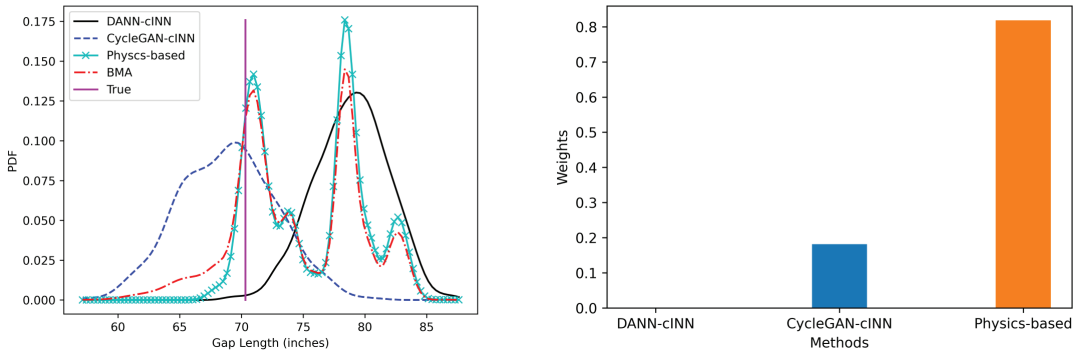

Fig. 22 Bayesian model averaging of posterior distributions (Case 1)

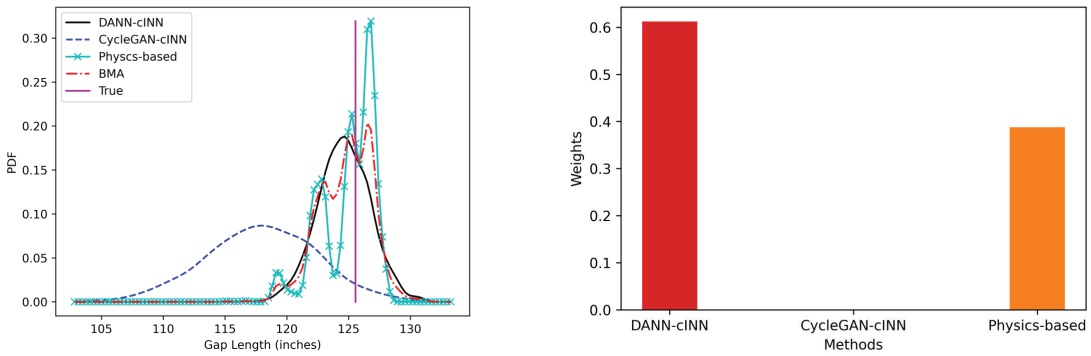

Fig. 23 Bayesian model averaging of posterior distributions (Case 2)

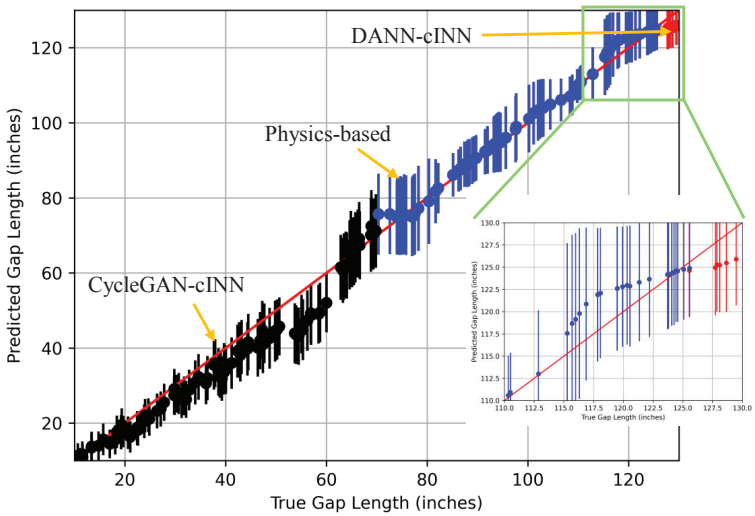

Fig. 24 Errorbar plot of the posterior distribution of different gap lengths after model selection using Bayes factor

ference. By transforming observations into a common domain and employing Bayesian model averaging, BiEDT leverages both physics-based models and advanced machine learning techniques to enhance the accuracy and reliability of damage state estimations for miter gates. The method not only combines the strengths of different damage diagnostic approaches but also quantifies uncertainty in the damage estimates, making it a robust tool in structural health monitoring. The method presented in this paper tackles the challenge of damage diagnostics of miter gates by synthesizing multiple data sources: real-time structural monitoring of gates of interest with unknown damage status, historical data from similar but different miter gates, and predictive insights from physics-based computational simulation models.

Despite its numerous advantages, the BiEDT framework does have certain limitations that must be acknowledged. One key limitation is that the accuracy of the translations and Bayesian inference is heavily dependent on the assumptions and quality of the underlying machine learning models. Any mis-specifications or inaccura-

cies in these models could lead to biased or erroneous damage state estimations. Additionally, the domain translation models used in this framework may not always adequately handle the full range of diverse operational conditions encountered in real-world applications. Moreover, the current framework primarily focuses on miter gates, and its application to other types of structures or systems has not been extensively validated. Future research could extend the BiEDT framework to a broader range of SHM scenarios, ensuring its adaptability and effectiveness across different domains.

In addition, an important issue to consider when applying the proposed framework is the assessment of the similarity between two miter gates. As been pointed out in Refs. [20,53], *negative transfer* occurs when utilizing data or knowledge from the source domain undesirably diminishes the learning performance in the target domain. It poses a long-standing challenge in transfer learning. Developing appropriate similarity metrics and determining a threshold to decide when the proposed framework can be applied and to avoid negative transfer is a research direction that worth studying in our future work. Another important area of future research involves the quantification of uncertainty in these machine learning models. Understanding and effectively managing this uncertainty is crucial for improving the reliability and confidence in the damage state estimations provided by the BiEDT framework. This could involve incorporating advanced methods of uncertainty quantification and exploring ways to integrate this uncertainty into the overall decision-making process [54].

Acknowledgment

This work was partially supported by the US Army Corps of Engineers through the U.S. Army Engineer Research and Development Center Research Cooperative Agreement W9132T-22-20014 and the U.S. National Science Foundation under Grant CMMI-2423521. The support is gratefully acknowledged. Any opinions, findings, or conclusions in this paper are those of the authors and do not necessarily reflect the sponsors' views. The authors would also like to thank Dr. Jice Zeng for helping set up the initial BayesFlow codes.

References

[1] Foltz, S. D., 2017, *Investigation of mechanical breakdowns leading to lock closuresInvestigation of mechanical breakdowns leading to lock closures*, Construction Engineering Research Laboratory (U.S.) Engineer Research and Development Center (U.S.).

[2] Eick, B. A., Treece, Z. R., Spencer Jr, B. F., Smith, M. D., Sweeney, S. C., Alexander, Q. G., and Foltz, S. D., 2018, "Automated damage detection in miter gates of navigation locks," Structural Control and Health Monitoring, **25**(1), p. e2053.

[3] Wang, Z., Huang, H.-Z., and Du, X., 2010, "Optimal design accounting for reliability, maintenance, and warranty," Journal of Mechanical Design, **132**(1), pp. 011007–011015.

[4] Vega, M. A., Hu, Z., Fillmore, T. B., Smith, M. D., and Todd, M. D., 2021, "A Novel Framework for Integration of Abstracted Inspection Data and Structural Health Monitoring for Damage Prognosis of Miter Gates," Reliability Engineering & System Safety, **211**, p. 107561.

[5] Estes, A. C., Frangopol, D. M., and Foltz, S. D., 2004, "Updating reliability of steel miter gates on locks and dams using visual inspection results," Engineering Structures, **26**(3), pp. 319–333.

[6] Liu, X. and Wang, P., 2022, "Valuation of continuous monitoring systems for engineering system design in recurrent maintenance decision scenarios," Journal of Mechanical Design, **144**(9), p. 091702.

[7] Chadha, M., Hu, Z., Farrar, C. R., and Todd, M. D., 2024, "Risk and Value informed Structural Health Monitoring system design for the miter gates," eJNDT, **29**(7).

[8] Nemani, V., Thelen, A., Hu, C., and Daining, S., 2023, "Degradation-aware ensemble of diverse predictors for remaining useful life prediction," Journal of Mechanical Design, **145**(3), p. 031706.

[9] Eick, B. A., Treece, Z. R., Spencer Jr, B. F., Smith, M. D., Sweeney, S. C., Alexander, Q. G., and Foltz, S. D., 2018, "Automated damage detection in miter gates of navigation locks," Structural Control and Health Monitoring, **25**(1), p. e2053, e2053 STC-16-0245.R2.

[10] *SMART GATE2007*, https://www.erdc.usace.army.mil/Media/Fact-Sheets/Fact-Sheet-Article-View/Article/476668/smart-gate/

[11] Vistasp M. Karbhari, F. A., 2009, *Structural Health Monitoring of Civil Infrastructure Systems*, Woodhead Publishing Series in Civil and Structural Engineering.

[12] Thelen, A., Zhang, X., Fink, O., Lu, Y., Ghosh, S., Youn, B. D., Todd, M. D., Mahadevan, S., Hu, C., and Hu, Z., 2022, "A comprehensive review of digital twin—part 1: modeling and twinning enabling technologies," Structural and Multidisciplinary Optimization, **65**(12), p. 354.

[13] Ramancha, M. K., Vega, M. A., Conte, J. P., Todd, M. D., and Hu, Z., 2022, "Bayesian model updating with finite element vs surrogate models: Application to a miter gate structural system," Engineering Structures, **272**, p. 114901.

[14] Levine, N., Golecki, T., Gomez, F., Eick, B., and Spencer, B. F., 2023, "Bayesian model updating of concrete-embedded miter gate anchorages and implications for design," Structural and Multidisciplinary Optimization, **66**(3), p. 60.

[15] Qian, G., Wu, Z., Hu, Z., and Todd, M. D., 2024, "Pitting corrosion diagnostics and prognostics for miter gates using multiscale simulation and image inspection data," Structural Health Monitoring, p. 14759217241264291.

[16] Qian, G., Zeng, J., Hu, Z., and Todd, M., 2024, "Bayesian Model Updating of Multiscale Simulations Informing Corrosion Prognostics Using Conditional Invertible Neural Networks," ASCE-ASME J Risk and Uncert in Engrg Sys Part B Mech Engrg, pp. 1–33.

[17] Zeng, Y., Zeng, J., Todd, M., and Hu, Z., 2024, "Data Augmentation Based on Image Translation for Bayesian Inference-Based Damage Diagnostics of Miter Gates," ASCE-ASME J Risk and Uncert in Engrg Sys Part B Mech Engrg, pp. 1–62.

[18] Bull, L. A., Gardner, P. A., Gosliga, J., Rogers, T. J., Dervilis, N., Cross, E. J., Papatheou, E., Maguire, A., Campos, C., and Worden, K., 2021, "Foundations of population-based SHM, Part I: Homogeneous populations and forms," Mechanical systems and signal processing, **148**, p. 107141.

[19] Gosliga, J., Gardner, P., Bull, L., Dervilis, N., and Worden, K., 2021, "Foundations of Population-based SHM, Part II: Heterogeneous populations–Graphs, networks, and communities," Mechanical Systems and Signal Processing, **148**, p. 107144.

[20] Gardner, P., Bull, L., Gosliga, J., Dervilis, N., and Worden, K., 2021, "Foundations of population-based SHM, Part III: Heterogeneous populations–Mapping and transfer," Mechanical Systems and Signal Processing, **149**, p. 107142.

[21] Whalen, E. and Mueller, C., 2022, "Toward reusable surrogate models: Graph-based transfer learning on trusses," Journal of Mechanical Design, **144**(2), p. 021704.

[22] Huang, X., Xie, T., Wang, Z., Chen, L., Zhou, Q., and Hu, Z., 2022, "A transfer learning-based multi-fidelity point-cloud neural network approach for melt pool modeling in additive manufacturing," ASCE-ASME Journal of Risk and Uncertainty in Engineering Systems, Part B: Mechanical Engineering, **8**(1), p. 011104.

[23] Venkateswara, H. and Panchanathan, S., 2020, *Introduction to Domain Adaptation*, Springer International Publishing, Cham, pp. 3–21.

[24] Chun, P.-j. and Kikuta, T., 2024, "Self-training with Bayesian neural networks and spatial priors for unsupervised domain adaptation in crack segmentation," Computer-Aided Civil and Infrastructure Engineering, **39**(17), pp. 2642–2661.

[25] Chen, Z., Wang, C., Wu, J., Deng, C., and Wang, Y., 2023, "Deep convolutional transfer learning-based structural damage detection with domain adaptation," Applied Intelligence, **53**(5), pp. 5085–5099.

[26] Huang, C.-G., Zhu, J., Han, Y., and Peng, W., 2022, "A Novel Bayesian Deep Dual Network With Unsupervised Domain Adaptation for Transfer Fault Prognosis Across Different Machines," IEEE Sensors Journal, **22**(8), pp. 7855–7867.

[27] Li, J. and He, D., 2020, "A Bayesian Optimization AdaBN-DCNN Method With Self-Optimized Structure and Hyperparameters for Domain Adaptation Remaining Useful Life Prediction," IEEE Access, **8**, pp. 41482–41501.

[28] Kwak, M. and Lee, J., 2023, "Diagnosis-based domain-adaptive design using designable data augmentation and Bayesian transfer learning: Target design estimation and validation," Applied Soft Computing, **143**, p. 110459.

[29] Xi, Z., 2019, "Model-based reliability analysis with both model uncertainty and parameter uncertainty," Journal of Mechanical Design, **141**(5), p. 051404.

[30] Zeng, Y., Zeng, J., Todd, M., and Hu, Z., 2024, "Augmenting Bayesian Inference-Based Damage Diagnostics of Miter Gates Based on Image Translation," *International Design Engineering Technical Conferences and Computers and Information in Engineering Conference*, American Society of Mechanical Engineers.

[31] Jiang, C., Vega, M. A., Ramancha, M. K., Todd, M. D., Conte, J. P., Parno, M., and Hu, Z., 2022, "Bayesian calibration of multi-level model with unobservable distributed response and application to miter gates," Mechanical Systems and Signal Processing, **170**, p. 108852.

[32] Hu, Z., Mourelatos, Z. P., Gorsich, D., Jayakumar, P., and Majcher, M., 2020, "Testing design optimization for uncertainty reduction in generating off-road mobility map using a Bayesian approach," Journal of Mechanical Design, **142**(2), p. 021402.

[33] Zhu, J.-Y., Park, T., Isola, P., and Efros, A. A., 2017, "Unpaired image-to-image translation using cycle-consistent adversarial networks," *Proceedings of the IEEE international conference on computer vision*, pp. 2223–2232.

[34] Zhu, J., Park, T., Isola, P., and Efros, A. A., 2017, "Unpaired Image-to-Image Translation using Cycle-Consistent Adversarial Networks," CoRR, **abs/1703.10593**.

[35] Ganin, Y., Ustinova, E., Ajakan, H., Germain, P., Larochelle, H., Laviolette, F., Marchand, M., and Lempitsky, V., 2016, "Domain-Adversarial Training of Neural Networks," 1505.07818, https://arxiv.org/abs/1505.07818

[36] Papamakarios, G., Nalisnick, E., Rezende, D. J., Mohamed, S., and Lakshminarayanan, B., 2021, "Normalizing flows for probabilistic modeling and inference," Journal of Machine Learning Research, **22**(57), pp. 1–64.

[37] Kobyzev, I., Prince, S. J., and Brubaker, M. A., 2020, "Normalizing flows: An introduction and review of current methods," IEEE transactions on pattern analysis and machine intelligence, **43**(11), pp. 3964–3979.

[38] Noori, M., Yuan, F.-G., and Farsangi, E. N., 2023, *Data-Centric Structural Health Monitoring: Mechanical, Aerospace and Complex Infrastructure Systems*, Walter de Gruyter GmbH & Co KG.
[39] Zeng, J., Todd, M. D., and Hu, Z., 2023, "Probabilistic damage detection using a new likelihood-free Bayesian inference method," Journal of Civil Structural Health Monitoring, **13**(2), pp. 319–341.
[40] Ardizzone, L., Kruse, J., Wirkert, S., Rahner, D., Pellegrini, E. W., Klessen, R. S., Maier-Hein, L., Rother, C., and Köthe, U., 2018, "Analyzing inverse problems with invertible neural networks," arXiv preprint arXiv:1808.04730.
[41] Radev, S. T., Mertens, U. K., Voss, A., Ardizzone, L., and Köthe, U., 2020, "BayesFlow: Learning complex stochastic models with invertible neural networks," IEEE transactions on neural networks and learning systems, **33**(4), pp. 1452–1466.
[42] Ardizzone, L., Lüth, C., Kruse, J., Rother, C., and Köthe, U., 2019, "Guided image generation with conditional invertible neural networks," arXiv preprint arXiv:1907.02392.
[43] Dinh, L., Sohl-Dickstein, J., and Bengio, S., 2016, "Density estimation using real nvp," arXiv preprint arXiv:1605.08803.
[44] Ardizzone, L., Kruse, J., Lüth, C., Bracher, N., Rother, C., and Köthe, U., 2021, "Conditional invertible neural networks for diverse image-to-image translation," *Pattern Recognition: 42nd DAGM German Conference, DAGM GCPR 2020, Tübingen, Germany, September 28–October 1, 2020, Proceedings 42*, Springer, pp. 373–387.
[45] Hu, Z., Hu, C., Mourelatos, Z. P., and Mahadevan, S., 2019, "Model discrepancy quantification in simulation-based design of dynamical systems," Journal of Mechanical Design, **141**(1), p. 011401.
[46] Thelen, A., Zhang, X., Fink, O., Lu, Y., Ghosh, S., Youn, B. D., Todd, M. D., Mahadevan, S., Hu, C., and Hu, Z., 2023, "A comprehensive review of digital twin—part 2: roles of uncertainty quantification and optimization, a battery digital twin, and perspectives," Structural and multidisciplinary optimization, **66**(1), p. 1.
[47] Hu, Z., Hu, C., and Hu, W., 2024, "A tutorial on digital twins for predictive maintenance," Structural Health Monitoring/Management (SHM) in Aerospace Structures, pp. 453–501.
[48] Jiang, Z., Li, W., Apley, D. W., and Chen, W., 2015, "A spatial-random-process based multidisciplinary system uncertainty propagation approach with model uncertainty," Journal of Mechanical Design, **137**(10), p. 101402.
[49] Jiang, C., Hu, Z., Liu, Y., Mourelatos, Z. P., Gorsich, D., and Jayakumar, P., 2020, "A sequential calibration and validation framework for model uncertainty quantification and reduction," Computer Methods in Applied Mechanics and Engineering, **368**, p. 113172.
[50] Apley, D. W., Liu, J., and Chen, W., 2006, "Understanding the effects of model uncertainty in robust design with computer experiments," Journal of Mechanical Design, **128**(4), pp. 945–958.
[51] Radev, S. T., Schmitt, M., Pratz, V., Picchini, U., Köthe, U., and Bürkner, P.-C., 2023, "JANA: Jointly amortized neural approximation of complex Bayesian models," *Uncertainty in Artificial Intelligence*, PMLR, pp. 1695–1706.
[52] Radev, S. T., Schmitt, M., Schumacher, L., Elsemüller, L., Pratz, V., Schälte, Y., Köthe, U., and Bürkner, P.-C., 2023, "Bayesflow: Amortized bayesian workflows with neural networks," arXiv preprint arXiv:2306.16015.
[53] Zhang, W., Deng, L., Zhang, L., and Wu, D., 2023, "A Survey on Negative Transfer," IEEE/CAA Journal of Automatica Sinica, **10**(2), p. 305–329.
[54] Nemani, V., Biggio, L., Huan, X., Hu, Z., Fink, O., Tran, A., Wang, Y., Zhang, X., and Hu, C., 2023, "Uncertainty quantification in machine learning for engineering design and health prognostics: A tutorial," Mechanical Systems and Signal Processing, **205**, p. 110796.

List of Figures

List of Tables